UNIVERSITÀ DEGLI STUDI DI MILANO

DIPARTIMENTO DI SCIENZE FARMACOLOGICHE E BIOMOLECOLARI

DOTTORATO IN SCIENZE FARMACOLOGICHE SPERIMENTALI E CLINICHE

XXIX CICLO

OSTEOPROTEGERIN AS A NEW POSSIBLE PLAYER IN MITRAL VALVE PROLAPSE WITH SEVERE REGURGITATION: FROM *IN VITRO* TO HUMAN STUDIES

BIO/14

Dott.ssa Paola SONGIA
Matricola R10599

TUTOR: Chiar.ma Prof.ssa Marina Camera
COTUTOR: Dott. Paolo Poggio
COORDINATORE: Chiar.mo Prof. Alberto Corsini

A.A.
2015-2016

ABSTRACT

Background: Mitral valve prolapse (MVP) is a common valve pathology and affects more than 176 million people worldwide. Echocardiography is the diagnostic gold standard and surgical intervention represents the only successful treatment when the prolapse causes severe regurgitation and symptoms occur. To date, there are no reliable biomarkers available for the identification of this pathology. MVP is a disorder characterized by extracellular matrix (ECM) remodelling but molecular and cellular mechanisms are not fully understood. The disruption of ECM tight regulation and the constitutive activation of valve interstitial cells (VIC) have been linked to MVP, as well as valve endothelial cell (VEC) mesenchymal transition (EndMT). Osteoprotegerin (OPG) is involved in a myriad of physiological and pathological processes. In the vascular environment, both endothelial and smooth muscle cells constitutively secrete OPG. In order to gain further insights into the molecular mechanisms involved in MVP progression, we investigated the role of OPG during EndMT and we generated a predictive model able to identify MVP patients with high accuracy.

Methods: Human VECs and VICs were isolated from posterior mitral valve leaflets of patients who underwent mitral valve repair. β-glycerolphosphate and ascorbic acid (βGAA) treatments were used to promote EndMT. Immunofluorescence, Western blot, quantitative and digital PCR were performed to evaluate VEC and VIC phenotypes. We assessed the oxidative stress status measuring the oxidized (GSSG) and the reduced (GSH) form of glutathione by liquid chromatography-tandem mass spectrometry method. OPG plasma levels were measured by enzyme-linked immunosorbent assay. These biochemical variables combined with clinical and demographic parameters were considered to generate a logistic regression model able to identify MVP patients with high sensitivity and specificity.

Results: OPG was significantly elevated (309±49.8%) in prolapsed tissues when compared to healthy tissues ($p<0.05$). We carried out an *in vitro* system able to force EndMT in isolated VECs. During EndMT, VECs showed a significant up-regulation of OPG RNA levels (4.1±1.3 fold *vs*. untreated cells; $p<0.05$). In addition, VECs secreted more OPG in comparison to untreated cells (2369±564.7 pg/µg and 923.5±261.1 pg/µg of total protein, respectively; $p<0.05$). Moreover, OPG itself triggered autocrine effects (RNA levels): collagen I (Col1A1, +4.0±0.6; $p<0.001$); collagen III (Col3A1, +3.0±0.6; $p<0.01$); bone morphogenetic protein 4 (BMP4, +2.4±0.7; $p<0.05$) and versican (VCAN, +3.8±0.2; $p<0.001$). Furthermore, OPG treatments accelerated VEC migration (area closed: 43.3±3.9% treated cells *vs*. 21.8±2.6% untreated cells; $p<0.001$). OPG also promoted VICs proliferation (22.4% increment;

p<0.05) and significantly up-regulated VIC RNA levels: Col1A1 (+2.24±0.29; p<0.001); Col3A1 (+1.58±0.29; p<0.05); BMP4 (+1.6±0.1; p<0.05); biglycan (BGN, +1.9±0.3; p <0.001); VCAN (+1.5±0.2; p <0.05); metalloproteinase 2 (MMP2, +1.6±0.1; p <0.01); smooth muscle actin (SMA, +1.6±0.2); and OPG (+1.5±0.2; p<0.05).

Regarding plasma analyses, both oxidative stress (GSSG/GSH ratio) and OPG levels were significantly higher in patients compared to control subjects (0.116±0.007 *vs.* 0.053±0.013 and 1748±100.2 *vs.* 1109±45.3 pg/mL, respectively; p<0.001). Finally, the combination of these two variables with body-mass index allowed us to generate a regression model able to correctly identify 95% of patients and 90% of control subjects.

Conclusions: Our results support EndMT as a possible mechanism involved in the pathogenesis of mitral valve degeneration. In addition, to the best of our knowledge, this is the first study to show a strong association between OPG, oxidative stress status and body-mass index in patients affected by MVP with severe regurgitation. Finally, since it is quite hard to believe that one single protein could discriminate two populations with high specificity and sensitivity, we believe that this approach could improve the identification of several signatures not only in mitral valve disease. As the mechanisms explaining these correlations are still unclear, further molecular studies along with clinical validations will be necessary to confirm our findings.

RIASSUNTO

Introduzione: Il prolasso della valvola mitralica è una diffusa patologia valvolare che affligge più di 176 milioni di persone nel mondo. Nella pratica clinica, l'ecocardiografia è lo strumento diagnostico di riferimento e l'intervento chirurgico rappresenta il solo trattamento efficace quando il prolasso causa rigurgito severo. Inoltre, ad oggi, non esistono biomarcatori circolanti utili per l'identificazione di tale patologia. Alterazioni a carico delle matrice extracellulare, come l'attivazione costitutiva delle cellule interstiziali e l'acquisizione da parte delle cellule endoteliali di un fenotipo mesenchimale (EndMT), svolgono un ruolo chiave nello sviluppo del prolasso mitralico. Tuttavia, ulteriori studi risultano necessari per una conoscenza più approfondita dei meccanismi molecolari e cellulari alla base di tale patologia. Inoltre è noto che l'osteoprotegerina (OPG), una glicoproteina coinvolta in numerosi processi patologici e fisiologici, viene rilasciata costitutivamente sia dalle cellule muscolari che endoteliali. Lo scopo dello studio è la valutazione del possibile ruolo dell'OPG durante l'EndMT e la creazione di un modello predittivo in grado di identificare con elevata accuratezza i pazienti affetti da prolasso mitralico.

Metodi: Le cellule endoteliali e interstiziali sono state isolate dai lembi mitralici posteriori, ottenuti da pazienti sottoposti ad un intervento di riparazione della valvola mitralica. Allo scopo di indurre EndMT, le cellule endoteliali sono state trattate con β-glicerolofosfato e acido ascorbico. Tecniche di immunofluorescenza, elettroforesi, PCR quantitativa e digitale sono state impiegate per analizzare le caratteristiche fenotipiche di entrambi i tipi cellulari. Inoltre, mediante un metodo di cromatografia liquida accoppiato alla spettrometria di massa, è stato possibile misurare i livelli della forma ossidata (GSSG) e ridotta (GSH) del glutatione, il cui rapporto è un indice riconosciuto di stress ossidativo. Parallelamente, le concentrazioni plasmatiche di OPG sono state valutate mediante saggio ELISA. La combinazione di queste variabili biochimiche con parametri clinici e demografici, è stata presa in considerazione per la generazione di un modello statistico in grado di identificare con elevata sensitività e specificità pazienti affetti da prolasso mitralico.

Risultati: Nei tessuti ottenuti dai pazienti con prolasso mitralico, i livelli di espressione dell'OPG risultavano significativamente più elevati (309±49.8%; $p<0.05$) rispetto a quelli riscontrati nei tessuti ottenuti da soggetti sani. Successivamente abbiamo messo a punto un sistema *in vitro* in grado di promuovere l'EndMT delle cellule endoteliali isolate da pazienti. Durante l'EndMT, le cellule endoteliali mostravano sia un significativo aumento dei livelli di RNA per l'OPG (aumento di 4.1±1.3 volte *vs*. cellule non trattate; $p<0.05$) che una maggiore produzione di OPG (2369±564.7 pg/μg e 923.5±261.1 pg/μg di proteine totali, rispettivamente;

p<0.05) rispetto alle cellule non trattate. L'OPG a sua volta determinava un aumento dei livelli di RNA per il collagene I (Col1A1, +4.0±0.6; p<0.001); il collagene III (Col3A1, +3.0±0.6; p<0.01); la proteina morfo-genetica dell'osso 4 (BMP4, +2.4±0.7; p<0.05) e il versicano (VCAN, +3.8±0.2; p<0.001). In aggiunta, le cellule endoteliali trattate con OPG migravano più velocemente rispetto a quelle non trattate (area di chiusura: 43.3±3.9% cellule trattate *vs.* 21.8±2.6% cellule non trattate; p<0.001). Per quanto riguarda le cellule interstiziali, l'OPG ne promuoveva la proliferazione (incremento pari al 22.4%; p<0.05) e un aumento statisticamente significativo dei livelli di RNA per il Col1A1 (+2.24±0.29; p<0.001); il Col3A1 (+1.58±0.29; p<0.05); la BMP4 (+1.6±0.1; p<0.05); il biglicano (BGN, +1.9±0.3; p <0.001); il VCAN (+1.5±0.2; p <0.05); la metalloproteasi 2 (MMP2, +1.6±0.1; p <0.01); l'actina del muscolo liscio (SMA, +1.6±0.2); e l'OPG stessa (+1.5±0.2; p<0.05). Inoltre, i livelli di stress ossidativo (rapporto GSSG/GSH) e i livelli plasmatici dell'OPG risultavano significativamente più elevati nei pazienti rispetto a soggetti sani (0.116±0.007 *vs.* 0.053±0.013 e 1748±100.2 pg/mL *vs.* 1109±45.3 pg/mL, rispettivamente; p<0.001). Combinando queste due variabili con l'indice di massa corporea (BMI) è stato possibile ottenere un modello di regressione logistica in grado di identificare correttamente il 95% dei pazienti e il 90% dei soggetti controllo.

Conclusioni: I risultati ottenuti confermano che l'EndMT è un possibile meccanismo coinvolto nella patogenesi della degenerazione della valvola mitralica, inoltre per la prima volta, nei pazienti affetti da prolasso mitralico con rigurgito severo, è stata evidenziata una stretta associazione tra OPG, stress ossidativo e BMI. Tuttavia, i meccanismi alla base di tale associazione sono ancora poco chiari e di conseguenza si rendono necessari ulteriori studi molecolari e validazioni cliniche, per confermare i nostri risultati. Dal momento che risulta difficile poter distinguere correttamente due popolazioni considerando una sola variabile, riteniamo che la combinazione di più variabili possa essere d'aiuto per l'identificazione di nuove "firme molecolari", non solo per le malattie a carico della valvola mitralica, ma anche per altre patologie.

ABBREVIATIONS

BMI = body-mass index

BMP4 = bone morphogenetic protein 4

CD31 = platelet endothelial cell adhesion molecule

Col1A1 = collagen I A1

Col3A1 = collagen III A1

dPCR = digital PCR

ECM = extracellular matrix

EndMT = endothelial mesenchymal transition

GSH = reduced glutathione

GSSG = oxidized glutathione

MMPs = metalloproteinases

MR = mitral regurgitation

MVP = mitral valve prolapse

OPG = osteoprotegerin

qPCR = quantitative qPCR

SMA= α-smooth muscle actin

VCAN = versican

VECs = valve endothelial cells

VICs = valve interstitial cells

VIM = vimentin

βGAA = β-glycerolphosphate and ascorbic acid

SDCs = syndecan receptors

ERK = extracellular signal-regulated kinase

GAPDH = glyceraldehyde 3-phosphate dehydrogenase

Hep I = heparinase I

BGN = biglycan

CTRL = control subjects

1. INTRODUCTION

1.1 The Heart

The heart is a specialized muscle responsible for pumping blood to the entire body. It is surrounded by a fibrous sac, the epicardium, and is positioned in the thoracic cavity. The heart is divided into a left and a right side by the septal wall and each side consists of two muscular chambers: the atrium and the ventricle (**Figure 1.1**). The right side of the heart pumps deoxygenated blood in the lungs (pulmonary circulation) while the left side delivers oxygen-rich blood to the body (systemic circulation). In particular, the systemic deoxygenated blood through the superior and inferior vena cava arrives in the right atrium and then it is directed to the right ventricle. From this ventricle, the blood reach the lungs through the pulmonary artery. The oxygenated blood returns to the left atrium of the heart from the four pulmonary veins and it is directed into the left ventricle. This last chamber pumps the oxygenated blood into the systemic circulation towards the aorta.

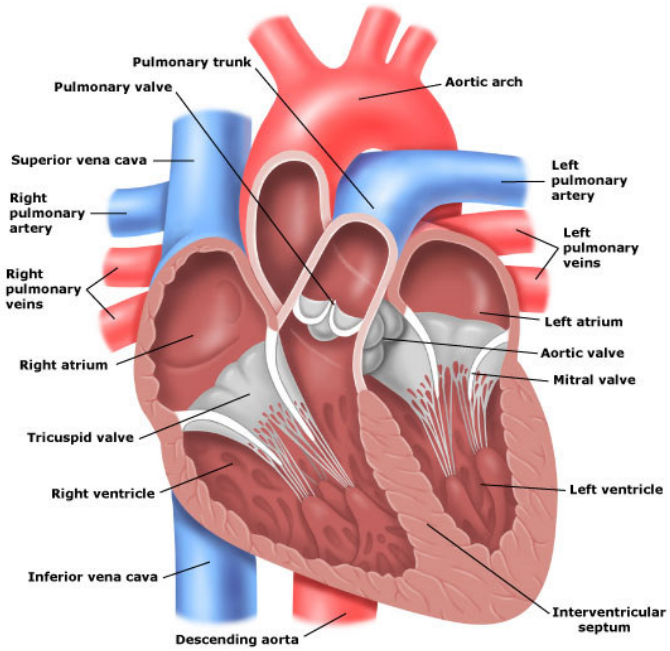

Figure 1.1 Illustration of the anatomy of the human heart. Adapted from http://nursingmedic.blogspot.com/2010/11/anatomy-of-heart.html

The four cardiac valves ensure the unidirectional blood flow within the heart. The atrioventricular (AV) valves, tricuspid and mitral, separate the atria from the ventricles on the right and left sides, respectively. Instead, the pulmonary and aortic valves, also known as semilunar valves, separate the ventricles from the great arteries.

1.1.1 The Cardiac Cycle

Myocardial contraction is due to a spontaneous generation of an electrical impulse. The impulse starts in the sinus node located in the superior lateral wall of the right atrium. The cardiac cycle, a sequence of mechanical and electrical events, mainly consists of four phases: atrial contraction (inflow), isovolumetric ventricular contraction, ejection (outflow) and isovolumetric ventricular relaxation. Commonly, these phases are also known as: systole and diastole. The systolic phase refers to ventricular contraction, while, the diastolic phase refers to ventricular relaxation (**Figure 1.2**).

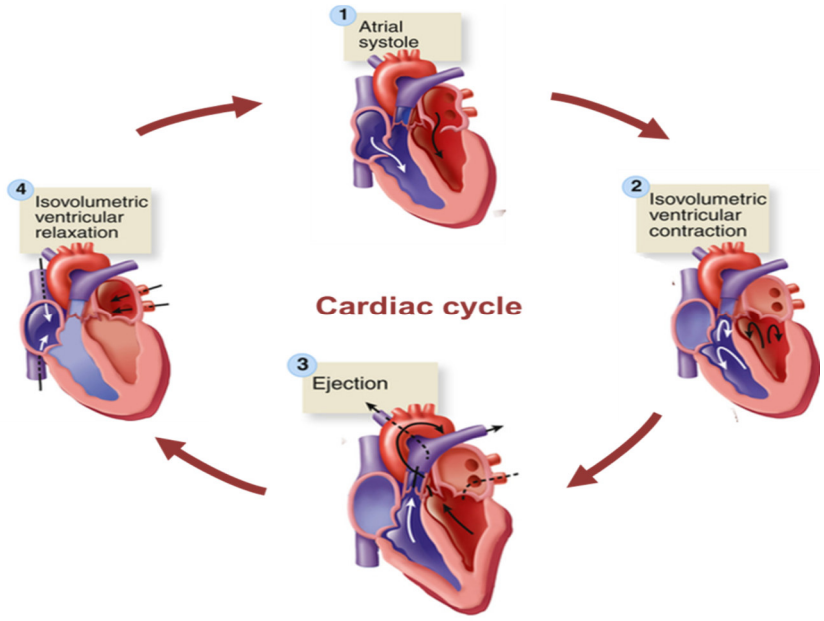

Figure 1.2 Cardiac cycle. The cardiac cycle can be mainly divided in four phases: 1) atrial systole, 2) isovolumetric ventricular contraction, 3) ejection and 4) isovolumetric ventricular relaxation. Adapted from Patton KT, Thibodeau GA: Anatomy & physiology, ed. 8, St Louis, 2013.

The cardiac cycle has an average time of 800 ms and the cardiac valves open and close approximately 40 million times a year, and more than 3 billion times during the average human lifetime [1].

1.2 Mitral Valve

1.2.1 Structure and Function

The mitral valve is located between the left atrium and the left ventricle. It is a complex apparatus made up of several structures: the mitral annulus, the leaflets (anterior and posterior), the chordae tendineae and the papillary muscles (**Figure 1.3**). It is a dynamic three-dimensional system, which, by working in synchrony, allows left ventricular blood-inflow during diastole, whilst during systole the mitral valve isolates the left atrium from the left ventricle to ensure unidirectional blood-flow.

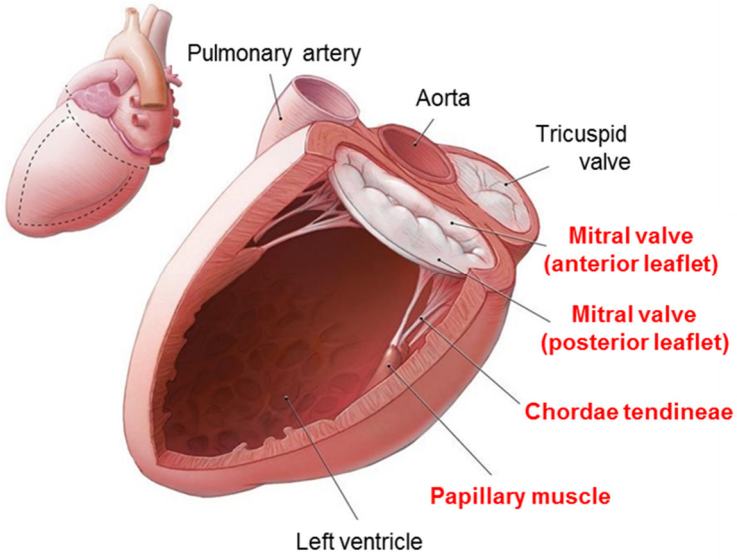

Figure 1.3 Components of mitral valve apparatus. The mitral valve is made up of several structures: the mitral annulus, the leaflets (anterior and posterior), the chordae tendineae and the papillary muscles. Adapted from http://emedicine.medscape.com/article/1878301-overview

Normal valve functioning is crucial and depends on its integrity since it regulates the blood flow within the two highest-pressure chambers. However, the possible alterations of mechanical and cellular integrity lead to an abnormal leaflet closure with blood regurgitation in the left atrium, which in turn, causes loss of ventricular pressure and forward flow.

The mitral valve has two leaflets: anterior and posterior. Both of them are attached to the mitral annulus at their basal ends, whereas multiple chordae tendineae emerge from the leaflet ventricular surfaces and attach distally to the papillary muscles. The anterior leaflet is characterized by a trapezoid- or dome shape and is anchored to one third of the annular circumference. In particular, it is attached to the fibrous portion of the mitral annulus and shares tissue continuity with the non-coronary leaflet of the aortic valve. The posterior leaflet is attached to two-thirds of the annular circumference.

Several nomenclatures are available for the mitral valve anatomy: Classic [2], Duran [3] and Carpentier [4]. The European Association of Echocardiography and the American Society of Echocardiography, when discuss the mitral valve anatomy, adopt the Carpentier's nomenclature. Accordingly, we implemented this classification. In particular, Carpentier's nomenclature (**Figure 1.4**) divides the anterior leaflet in three regions labeled A1, A2 and A3 corresponding to the adjacent regions of the posterior leaflet called P1, P2 and P3.

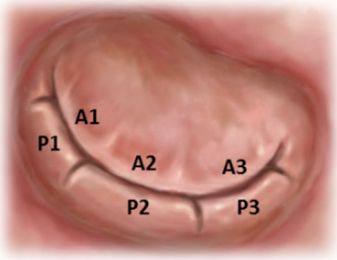

Figure 1.4 Carpentier's nomenclature of mitral valve leaflets. The anterior leaflets can be divided in three regions labeled A1, A2 and A3 corresponding to the adjacent regions of the posterior leaflet called lateral P1, P2 and P3. Adapted from Guy TS, Hill AC. Mitral valve prolapse. *Annu Rev Med*. 63:277-92; 2012.

The leaflets are a highly specialized structure (**Figure 1.5**). For each leaflet, it is possible to identify, from the attachment point at the annulus to the free edge, three different zones: basal, clear and rough. The **basal** zone contains nerve fibers and terminals that maintain electrophysiological continuity with the rest of the heart [5, 6]. The **clear** zone is characterized by a dense collagenous network and fibroblasts able to actively repair the extracellular matrix [7]. Finally, the **rough** zone, at the free edge of the leaflet, is thicker than the previous one and it is the main area of chordal attachment. It is also rich in glycosamiglaycans, which retaining water are capable of sustaining the compressive stress from coaptation [8].

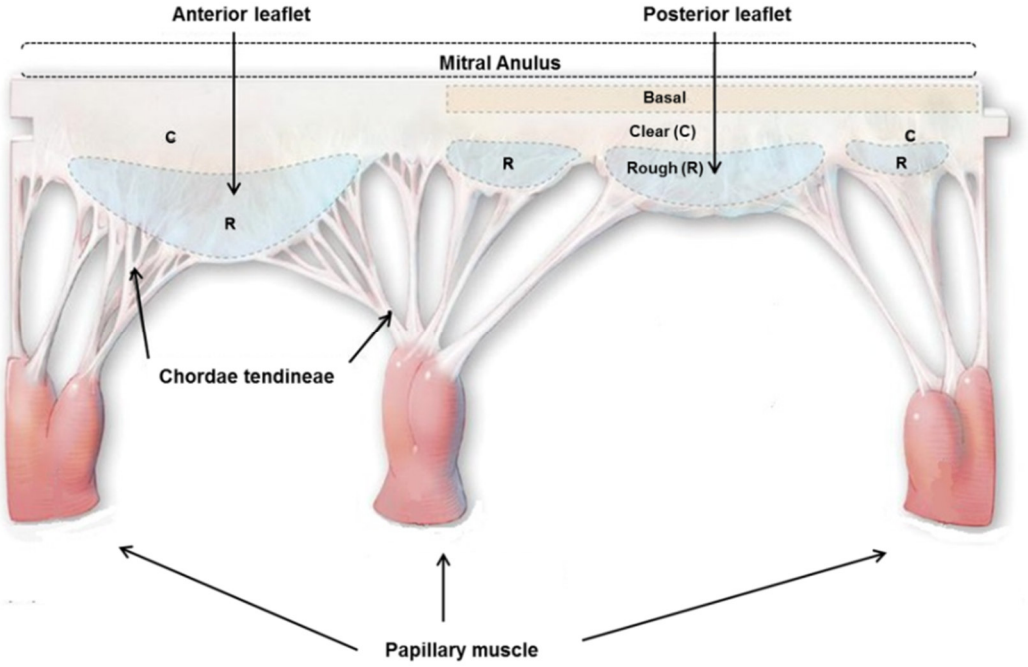

Figure 1.5 Basal, clear and rough zone of mitral valve leaflets. In each leaflet, it is possible to identify, from the attachment point at the annulus to the free edge, three different zones: basal, clear and rough. Adapted from http://emedicine.medscape.com/article/1878301-overview.

The mitral valve cross-sectional structure appears analogous to the aortic valve and three well-defined tissue layers could be identified: *atrialis*, *spongiosa* and *fibrosa* (**Figure 1.6**). Each layer has a different thickness, cell population, matrix composition and biomechanical features

that contribute to its proper function. The *atrialis* layer contains connective tissue that appears like a network of lamellar collagen and elastin. This network plays a pivotal role in adaptive responses to stress conditions [9]. The *spongiosa* is made up of glycosaminoglycans and loosely arranged collagen fibers [10]. Its main function is to support the compression between the outer layers, giving leaflet flexibility and attenuating the vibrations due to valve coaptation [11]. The last layer, *fibrosa,* is predominantly is made up of compact and aligned collagen fibers providing strength and stiffness to the leaflet. These fibers are also surrounded by glycosaminoglycans and proteoglycans in order to sustain compressive loading imposed by leaflet coaptation [8]. The layer distribution appears significantly different in the two leaflets. The thickness of the anterior one is due to a dominant *fibrosa* layer that helps to sustain tensile load without tissue disruption. The posterior leaflet appears thinner and more flexible compared with the anterior one [12].

Two cell types populate the mitral valve leaflets (**Figure 1.6**): 1) a monolayer of valve endothelial cells (VECs) which covers both the atrial and ventricular surface and 2) a heterogeneous population, called valve interstitial cells (VICs) that resides within the three layers. VECs provide a physical barrier against the hemodynamic environment. VICs represent the most abundant cell type within the valve and this dynamic cell population plays a pivotal role in the maintenance of normal leaflet architecture. In particular, VICs regulate extracellular matrix production and degradation during valve development and throughout the entire life [11, 13]. These two populations reciprocally interact to ensure normal cell homeostasis [14-17].

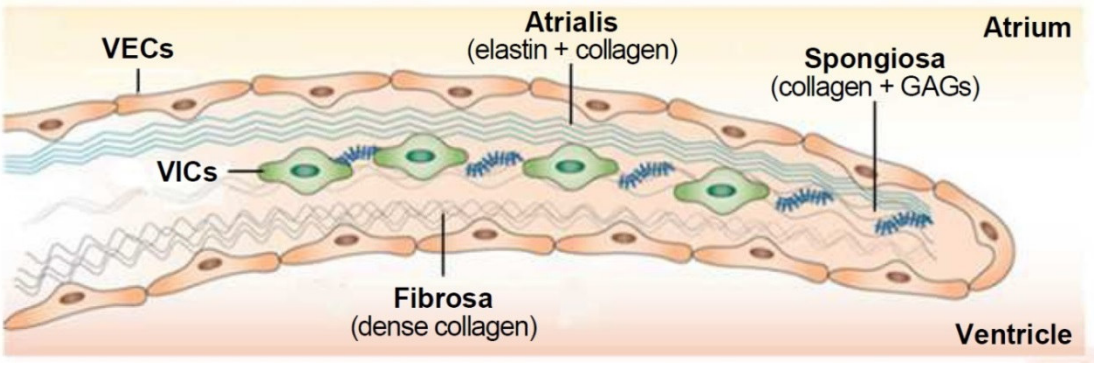

Figure 1.6 Mitral valve leaflet structure. The leaflets are organized in three different layers: *atrialis*, *spongiosa* and *fibrosa.* Endothelial cells cover both the atrial and ventricular surface while the interstitial cells are embedded within the layers. VECs: valve endothelial cells; VICs: valve interstitial cells; GAGs: glycosaminoglycans. Adapted from Levine RA *et al.* Mitral valve disease--morphology and mechanisms. Nat Rev Cardiol. 12(12):689-710; 2015.

1.3 Mitral Valve Diseases

Abnormalities in the mitral valve complex prevent normal leaflet coaptation and may cause blood regurgitation in the left atrium during systole. This pathological condition is known as mitral regurgitation (MR). MR due to structural or degenerative abnormalities is called *primary* MR, whereas, the *secondary* MR is a consequence of left ventricle alterations (such as myocardial infarction) [18, 19]. Another mitral disease, mostly common in elderly patients, is the mitral valve stenosis. It is characterized by a prominent calcification of mitral annulus and leaflets causing left ventricular inflow obstruction. This condition, however, is mainly caused by a rheumatic disease [19, 20].

1.3.1 Primary MR

Primary MR is mainly due to a degenerative mitral valve disease, defined as myxomatous degeneration characterized by distinctive histological changes with elongated and

redundant chordal apparatus [21]. Myxomatous mitral valve degeneration represents the principal cause of mitral valve prolapse (MVP) and it is one of the most common heart valve diseases in humans. MVP has a prevalence of 2-3% in the general population and affects more than 176 million people worldwide [11, 22]. Interestingly, the pathology is equally distributed between men and women [11] and patients with prolapse have significantly lower body-mass index (BMI) and waist-to-hip ratio than healthy subjects [22].

The prolapse may be identified when one, both, or a portion of the leaflets extend above the plane of the atrioventricular junction during left ventricular systole [23-25] causing blood flow regurgitation in the left atrium. It has been reported that prolapse involves the posterior leaflet in 67% of cases, the anterior one in 10% of cases and both leaflets in 23% of cases [26]. In the normal mitral valve, the ratio between anterior and posterior leaflet surface area is 2:1. However, this ratio appears altered in MVP due to an enlargement of all portions of the posterior leaflet. In addition, the myxomatous degeneration increases the mitral annular size and causes thinning, elongation and rupture of chordae tendineae [26-28].

In myxomatous MVP, increased expression of proteoglycans, which foster the leaflet thickening, and metalloproteinases (MMP), which contribute to the fragmentation of collagen and elastin fibers, disrupt the well-organized leaflet structure [29-32]. Indeed, Rabkin et *al.*[30] have observed an expansion of the *spongiosa*, strongly positive for proteoglycans, loosened collagen in the *fibrosa* and elastin fragmentation in *atrialis*. The authors have also identified an increased interstitial cell density in the spongiosa layer. These extracellular matrix changes were further confirmed by *Sainger et al.* [33] (**Figure 1.7**).

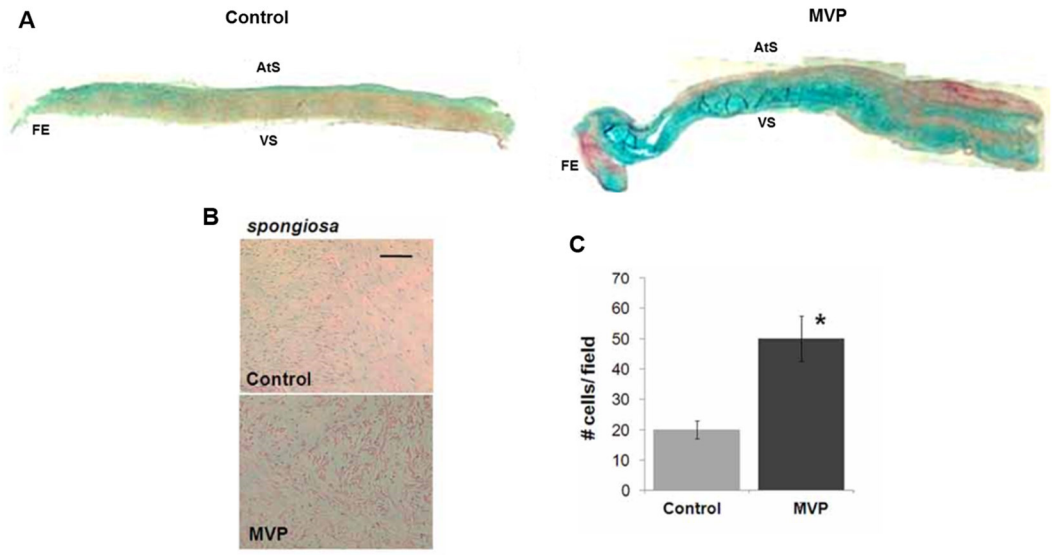

Figure 1.7 Morphological features of normal and myxomatous mitral valves. (**A**) Composite photomicrographs of sections of normal and diseased human mitral valve leaflets (transverse sections). Movat Pentachrome staining: proteoglycan (blue), collagen (yellow), muscle (red). FE, free edge; VS, ventricular surface; AtS, atrialis surface. (**B**) Representative image of Hematoxylin and Eosin staining (H&E) section of the mitral valve spongiosa layers of control and MVP patient and relative number of valve interstitial cells per field. (**C**) Quantification of total cell number within selected fields of the spongiosa layers. Bar graph: 50 μm *$p < 0.05$. Adapted from Sainger, R. *et al*. Human myxomatous mitral valve prolapse: role of bone morphogenetic protein 4 in valvular interstitial cell activation. J Cell Physiol, 227(6): 2595-604. 2012.

Another peculiar feature in MVP, is the VIC activation. In particular, VICs acquire a myofibroblast-like phenotype, characterized by increased expression of alpha-smooth muscle actin (SMA) [30, 34] (**Figure 1.8**).

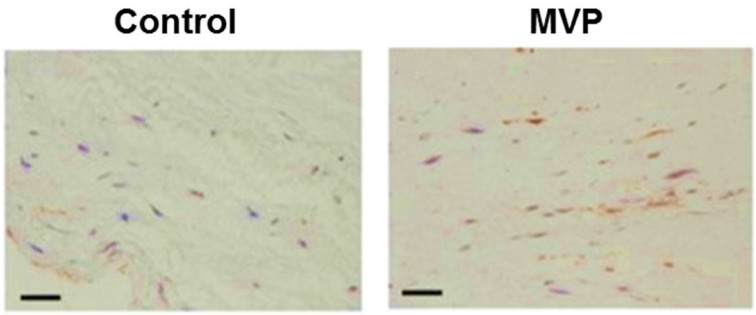

Figure 1.8 Accumulation of myofibroblast-like interstitial cells in myxomatous mitral valves. Interstitial cells acquire a myofibroblast-like phenotype characterized by of alpha-smooth muscle actin (SMA) espression. Scale bar 50 μm. Adapted from Rizzo, S. *et al*. TGF-beta1 pathway activation and adherens junction molecular pattern in nonsyndromic mitral valve prolapse. Cardiovasc Pathol, 24(6): 359-67; 2015.

The activated VICs are responsible for increased levels of different proteolytic enzymes, including MMPs, which are directly involved in collagen and elastin degradation. In particular, it has been reported that activated VICs express high levels of MMP-1, MMP-13 [30].

1.3.1.1 Barlow's vs. FED

In the 1980s, based on clinical patterns, echocardiography findings and gross surgical appearances [35], Carpentier classified the myxomatous degenerative mitral valve disease into two subtypes (**Table 1.1**). Barlow's disease (alternatively known as billowing mitral valve or diffuse myxomatous degeneration) is characterized by excessive and diffuse accumulation of glycosaminoglycans, whereas fibroelastic deficiency (FED) by extremely thin leaflets and chordae [35-39]. Echocardiography is currently the principal diagnostic tool used to distinguish Barlow's and FED. Patients with Barlow's disease often have a long clinical history of MR and are usually younger compared with FED. In contrast, FED patients experience chord rupture and flail leaflet [37, 38, 40].

Table 1.1 Macroscopic and microscopic characteristics of Barlow and FED diseases

	Barlow's Disease	FED Disease
Age at Diagnosis	< 50 years	> 50 years
Valve Morphology		
Annular Dilatation	(+++)	(+)
Leaflets	Thickened (++)	Thin
	Excess tissue (+++)	No excess tissue
Choardae	Heterogeneous	Thin
	Elongated	Ruptured
Lef ventricular dilatation	N/A	N/A

Macroscopically, Barlow's disease is characterized by thickened leaflets with a soft and gelatinous consistency, while, microscopically, the *fibrosa* appears expanded due to an alteration in the composition of glycosaminoglycans and proteoglycans. Collagen and elastic fibers appear fragmented and less dense than normal. In addition, the chordae tendineae are frequently characterized by myxomatous degeneration, which may represent the background for chordae rupture. Moreover, a superficial plaque is often observed, predominately on the ventricular side, characterized by the accumulation of stellate and spindle shaped cells. This plaque is a secondary feature, probably due to flow abnormalities [41] (**Figure 1.9A**).

In contrast, FED patients show a preserved three-layer leaflets structure. This pathological condition is characterized by decreased connective tissue, collagen, elastin and proteoglycans. The leaflets appear thin, smooth and translucent without excess tissue. Sometimes, a moderate mitral annulus dilatation and thin/elongated chordae may be found [11, 41] (**Figure 1.9B**). An important feature of FED is the myxomatous degeneration and thickening localized in focal areas within the flail scallop, mainly in the posterior leaflet (P2 segment) [39]. The etiology of connective tissue deficiency in FED patients is unknown but may be age-related.

The surgical approaches for Barlow's and FED disease are very different. It is not clear whether the Barlow's and FED are two histopathological features of the same syndrome or two genetically distinct entities.

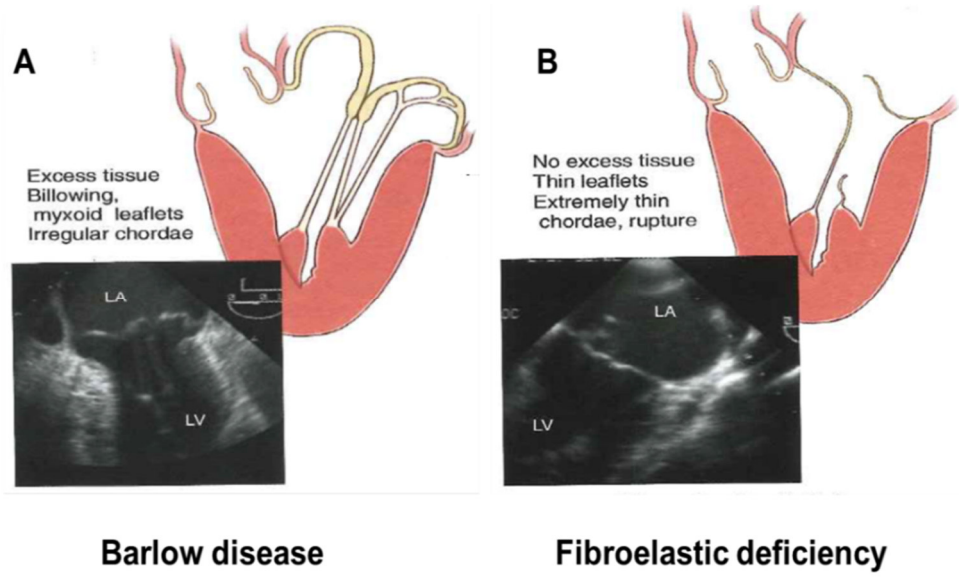

Figure 1.9. Morphological characteristics of Barlow and FED diseases. Adapted from Carpentier A. *et al.* Carpentier's Reconstructive Valve Surgery from Valve Analysis to Valve Reconstruction.

1.3.2 Secondary MR

Secondary MR is characterized by left ventricle dilatation that results in leaflet tethering and annular dilation preventing correct coaptation [42]. This pathological condition may be due to either ischemic or non-ischemic causes. Ischemic *secondary* MR is a consequence of myocardial infarction [43], while non-ischemic *secondary* MR is due to long lasting hypertension or idiopathic dilated cardiomyopathy [43].

Emerging evidence suggests a possible involvement of the endothelial to mesenchymal transition (EndMT) in the progression of MR [9, 44]. It is known that a subset of endothelial progenitor cells are able to undergo EndMT. In particular, during heart valve development, the

endothelial cells lose cell-cell contact, transiently upregulate SMA and migrate into the interstitium to populate the nascent valve; while in adult valves the EndMT may contribute to replenish the VIC population throughout the entire lifetime [45] (**Figure 1.10**).

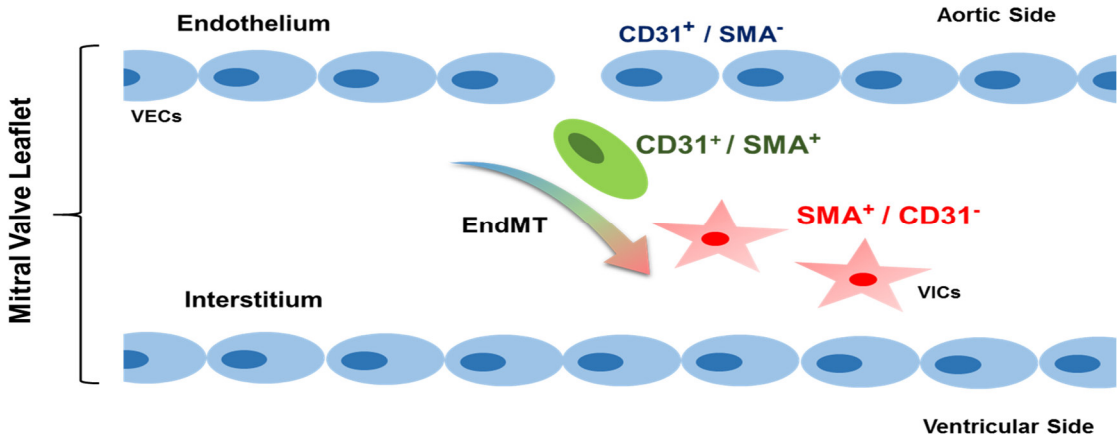

Figure 1.10 Endothelial to mesenchymal transition in mitral valve. Schematic representation of endothelial cell activation and their migration in the interstitium. CD31: platelet endothelial cell adhesion molecule; EndMT: endothelial to mesenchymal transition; SMA: α-smooth muscle actin; VECs: valve endothelial cells; VICs: valve interstitial cells.

In a recent work [9], ovine mitral valve leaflets were exposed to mechanical tethering, in order to mimic the mechanical stretch imposed on the mitral leaflets after myocardial infarction. Stretched leaflets showed positive staining for platelet endothelial cell adhesion molecule (CD31), an endothelial cell marker, and for SMA. The localization of SMA-positive cells, within and on the surface of the leaflets, represents not only the VIC activation but also that endothelial cells underwent EndMT [9].

These findings highlight that EndMT could be an adaptive mechanism that may contribute to increased mitral leaflet thickness and area, not only in secondary MR but also in the pathogenesis and progression of other mitral valve diseases.

1.3.3 Osteoprotegerin: a new player in mitral valve disease?

Osteoprotegerin (OPG) is a protein belonging to tumour necrosis factor (TNF) family. Several studies underlined a correlation between this protein and different pathological conditions such as coronary artery syndromes [46-48], aortic valve stenosis [49-51] and myocardial infarction [52], focusing only on the TNF superfamily. OPG is also linked to cardio-metabolic disorders [53] and increased cardiovascular and over-all mortality [54, 55]. It has been shown that transforming growth factor β (TGF-β), a well-known player in myxomatous MVP pathogenesis [56], increases oxidative stress status [57] as well as OPG production and secretion [58]. In the vasculature environment, both endothelial and smooth muscle cells constitutively secrete OPG [59, 60]. A recent study also highlighted the link between OPG and oxidative stress status on endothelial cells [61].

OPG, is a protein encoded by TNFRSF11B gene localized on 8q24.12 chromosome. It is a secretory glycoprotein composed of 401 aminoacids arranged into seven structural domains. In particular, cysteine rich domains (1-4) are essential for osteoclastogenesis inhibition, two death domains (5-6) which mediate apoptosis and an heparin binding domain (7) capable of interacting with heparin-sulphate proteoglycans (**Figure 1.11**).

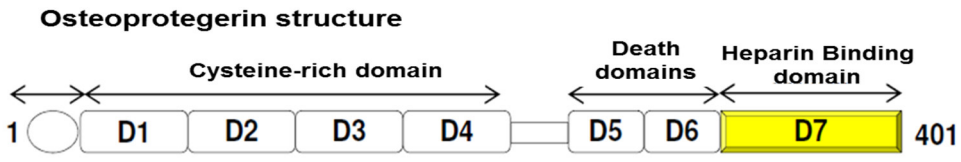

Figure 1.11 Osteoprotegerin structure. Protein of 401 aminoacids organized in seven structural domains.

OPG is mainly known as a decoy receptor for receptor activator of nuclear factor kappa-B ligand (RANKL) and tumour necrosis factor-related apoptosis-inducing ligand (TRAIL),

regulating different processes (*i.e.* bone resorption and cell apoptosis) (**Figure 1.12**). Interestingly, as previously reported, OPG may interact with heparin-sulphate proteoglycans, such as syndecan receptors. The syndecan family is made up of four isoforms expressed in different cell type and involved in many processes such as cell proliferation, differentiation, adhesion and migration [62] (**Figure 1.12**).

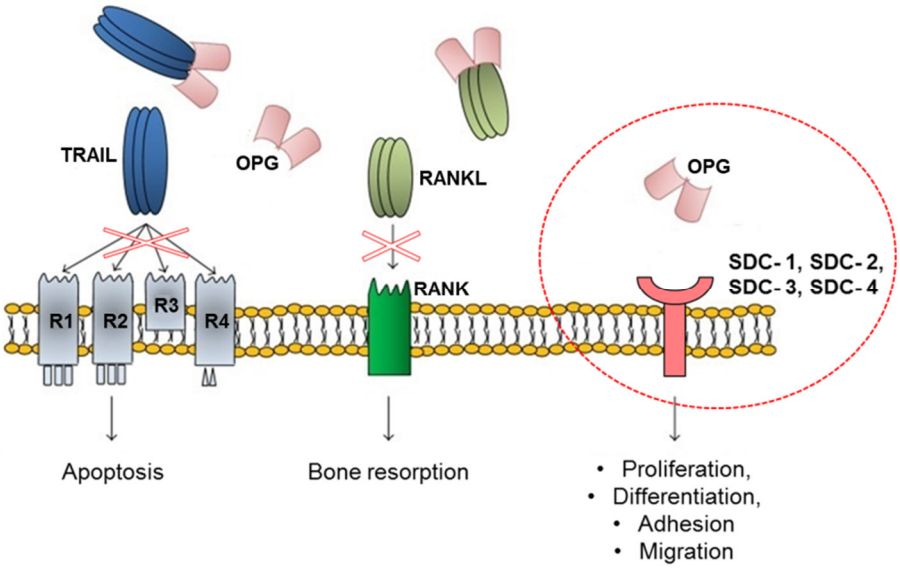

Figure 1.12 Schematic representation of OPG/TRAIL/RANKL/SYNDECAN system. OPG: osteoprotegerin; R: receptor; RANK: receptor activator of nuclear factor kappa-B; RANKL: receptor activator of nuclear factor kappa-B ligand; TRAIL: TNF-related apoptosis-inducing ligand. Adapted from Bernardi S. et al. Roles and Clinical Applications of OPG and TRAIL as Biomarkers in Cardiovascular Disease. *Biomed Res Int*. 2016. doi: 10.1155/2016/1752854.

1.3.4 Diagnosis

Two dimensional (2D) echocardiography represents the gold standard for diagnosis and assessment of patients presenting MR [18, 19]. It is a non-invasive imaging test able to provide detailed information about the structure and function of the mitral valve apparatus, the left ventricle and the atrium.

MVP represents a particular feature of mitral valve disease frequently associated with MR. During the echocardiographic evaluation, a single or bi-leaflet displacement, of at least 2 mm above the mitral annulus plane, define MVP. However, the diagnosis of MVP should also consider the evaluation of the structural changes of the entire mitral valve apparatus. A prolapse with leaflet thickening greater than 5 mm is defined 'classic', whereas a minor degree of thickening is regarded as 'non-classic' [63].

According to American guidelines [64], the regurgitated volume, evaluated through Doppler echocardiography, should also be taken into consideration in order to identify the severity of MR. In particular, a regurgitated volume of less than 30 mL/beat, between 30-60 mL/beat and more than 60 mL/beat corresponds to mild, moderate and severe MR, respectively [64, 65].

In current clinical practice, the use of three-dimensional (3D) echocardiographic (3DE) imaging represents a major innovation in cardiovascular ultrasound. Advancements in computer and transducer technologies make possible a real-time 3DE acquisition and allow the identification of cardiac structures from any spatial point of view [66]. The combination of 2D and 3D echocardiography provides detailed morphological and functional assessment, whereas Doppler echocardiography evaluates hemodynamics.

1.3.4.1 Biomarkers

Biomarkers have been defined by Hulka *et al.* [67] as "cellular, biochemical or molecular alterations that are measurable in biological media such as human tissues, cells, or fluids." To date, a broader definition has been proposed, taking into account all biological characteristics objectively measured as indicators of physiologic or pathologic processes [68]. In the clinical practice, they represent an important tool for a better diagnosis and prognosis of a specific pathological condition. Although, 2D echocardiography is the gold standard for MR diagnosis,

circulating biomarkers could provide valuable insights into the improvement of MVP patient stratification.

However, specific circulating biomarkers for MR have been investigated only in few studies and, in most cases, the investigators used animal models. In particular, in a recent study Deroyer *et al.*[69] have shown that apolipoprotein-A1 was an independent predictor of MR severity. It has also been shown that altered antioxidant defense systems and an increase of lipid peroxidation markers were disarranged in MVP patients, with severe MR, in comparison to healthy subjects [70]. Recently, a new class of circulating biomarkers, called non-coding RNAs, have emerged. In particular, microRNAs represent the most studied. Unfortunately, these circulating microRNAs have only been evaluated in canine models [71, 72]. Therefore, further studies, which may identify new specific molecular signatures, are needed to improve clinical practice.

1.4 Pharmacological and Surgical Treatments

1.4.1 Primary MR

To date, there are no recommended pharmacological treatments for patients with minimal symptom of *primary* MR or completely asymptomatic. Nevertheless, beta-blockers and angiotensin-converting enzyme inhibitors may be used for stress reduction on the valve [73], thus delaying surgical intervention. However, surgical intervention (repair or replacement) is the only available option when MR becomes severe or major symptoms occur [18, 19] .

Surgical repair has significant advantages in comparison to complete replacement. In particular, repair techniques offer lower operative mortality [74-78], preserve left ventricular function and give rise to fewer complications, such as thromboembolism, anticoagulant-related hemorrhage and endocarditis, [29, 75, 79-82]. According to the type and location of the mitral lesions, resection of the flail and prolapsed leaflet segment or reconstructive techniques, using

artificial chords, may be performed to treat *primary* MR [83]. The durability of mitral valve repair is higher for the posterior prolapse in comparison to the anterior and the bi-leaflet prolapse [84]. However, surgeons' expertise is very important for the long-term success of mitral repair and to guarantee low operative mortality rates (less than 1%) [18, 38]. The standard surgical approach, characterized by sternotomy under extracorporeal circulation and direct repair in according to Carpentier's method, is the treatment of choice. This method consists in a quadrangular or triangular resection of the prolapsed segment, chordal shortening, and ring replacement [85] (**Figure 1.13**).

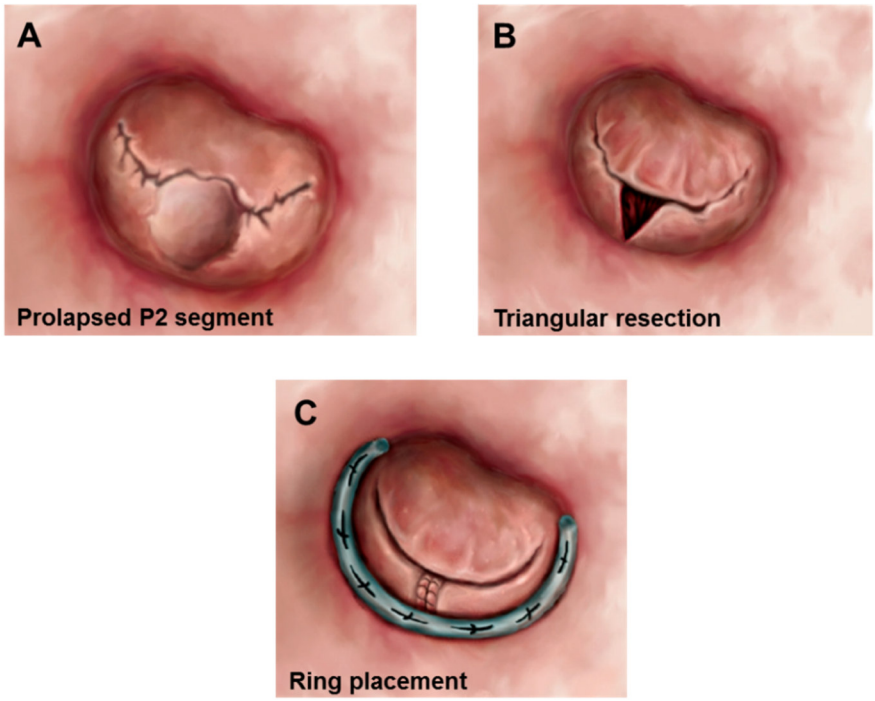

Figure 1.13 Mitral valve repair. (**A**) Typical anatomy associated with mitral valve regurgitation showing prolapse of the P2 segment of the posterior leaflet. (**B**) Triangular resection of prolapsed P2 segment. (**C**) Quadrangular resection and ring placement. Adapted from Guy TS, Hill AC. Mitral valve prolapse. *Annu Rev Med*. 63:277-92; 2012.

The standard surgical approach is not indicated for elderly patients with multiple co-morbidities [86, 87]. In this case, the surgeons use a minimally invasive technique without

extracorporeal circulation, known as percutaneous transcatheter mitral valve repair [86]. To date, several transcatheter devices are under investigation but the most adopted one is the MitraClip System [86]. Anterior and posterior leaflets are clipped together to create a double orifice within the mitral valve [86] (**Figure 1.14**).

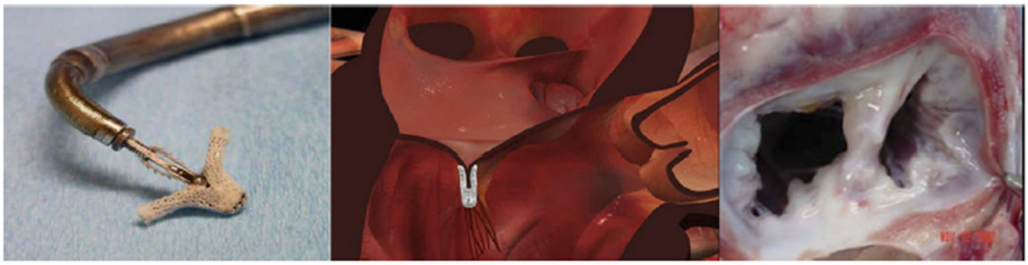

Figure 1.14 MitralClip device. MitraClip device (left), the MitraClip deployed on the mitral valve leaflets (middle), and a "double-orifice" within mitral valve (right). Adapted from Chiam P, Ruiz C. Percutaneous transcatheter mitral valve repair: a classification of the technology. JACC Cardiovasc Interv. 4(1):1-13; 2011.

The EVEREST II (Endovascular Valve Edge-to-Edge Repair Study) is a recent randomized trial that compared the MitralClip device to conventional surgery [88]. The study highlighted that patients treated with MitraClip had significant residual MR in comparison to standard surgery [88]. Nevertheless, the use of MitraClip is considered safer and results in similar clinical outcome improvements to standard surgery [88]. However, the results of a 5 year follow-up indicated the need of an additional surgery to correct residual MR in patients treated with Mitralclip [89]. Therefore, in the USA, the MitralClip is only approved for patients with *primary* MR and severe symptoms presenting a high risk for MV surgery. In Europe, however, the MitralClip can still be used at the surgeon's discretion [86].

1.4.2 Secondary MR

To date, the same pharmacological treatment recommended for left ventricular dysfunction (*i.e.* beta-blockers, angiotensin-converting enzyme inhibitors, angiotensin receptor antagonisms and aldosterone antagonisms) are the most effective available treatments for patients with *secondary* MR [18]. However, if patients are unresponsive to the medical treatments, surgical intervention is required.

The most common surgical approaches are mitral valve annuloplasty (repair) and replacement [43] but the best surgical treatment is still not clear [84]. Annuloplasty renews the correct leaflet coaptation, by reshaping the correct annular 3D structure, thus eliminating the acute mitral regurgitation symptoms [86]. Randomized trials [90, 91] have recently shown that clinical outcomes between repair and replacement in patients with *secondary* MR are equivalent. In addition, patients who underwent mitral replacement experienced a lower rate of MR recurrence, after 2 years, compared with those who underwent annuloplasty [90, 91]. In Europe, the *secondary* MR is the most common indication for MitralClip use. However, the system has the same limitations as previously described for *primary* MR.

2. AIMS

Mitral valve prolapse (MVP) is a debilitating disease with an estimated prevalence of 2-3% affecting more than 176 million people worldwide [11, 22]. The pathology was first described in the late 1800s [11], nevertheless, the major risk factors have not been identified yet [92]. The surgical intervention represents the only available option when the prolapse causes severe regurgitation and symptoms occur [18, 19]. The echocardiography is the diagnostic gold standard and, up to now, there are no reliable biomarkers available for the identification or the progression of this pathology.

MVP is a disorder characterized by extracellular matrix (ECM) remodeling. In particular, diseased mitral valves display an overexpression of bone morphogenetic proteins (*i.e*. BMP2 and 4), metalloproteinases (MMPs) and proteoglycans (*i.e.* biglycan and versican) [30, 33, 93]. A peculiar feature is the activation of valve interstitial cells (VIC). The activated VICs contribute to ECM alterations through an increase of proteolytic enzymes, including MMPs. Recently, MVP pathogenesis has been linked to valve endothelial cell (VEC) mesenchymal transition (EndMT) [9, 44]. Briefly, the endothelial cells lose their cell-cell contacts, acquire an activated phenotype and migratory properties. This process, in combination with ECM alterations, could be considered an adaptive mechanism that contributes to disease progression.

Osteoprotegerin (OPG) is a glycoprotein belonging to tumor necrosis factor family. In the vasculature environment, both endothelial and smooth muscle cells constitutively secrete OPG [59, 60]. OPG is a decoy receptor for receptor activator of nuclear factor kappa-B ligand (RANKL) and tumour necrosis factor-related apoptosis-inducing ligand (TRAIL), regulating multiple processes (*i.e.* bone resorption and cell apoptosis). OPG may also interacts with syndecan receptors, regulating other cellular processes (*i.e.* proliferation, differentiation and migration).

Given the background, the general aim of the study is to provide new details for the molecular mechanisms, underlying the disease progression. In particular, we evaluated EndMT in patients affected by mitral valve prolapse with severe regurgitation. Afterwards, we studied the potential involvement of OPG in EndMT and its effect(s) on mitral valve endothelial and interstitial cells. Finally, we investigated if OPG could be a potential circulating biomarker, in order to provide helpful insights for better MVP patient stratification. Therefore, the second aim was to generate a predictive model able to discriminate MVP patients from healthy subjects with high sensitivity and specificity.

3. MATERIALS AND METHODS

3.1 Patient Population

This observational study was approved by the Institutional Review Board of Centro Cardiologico Monzino IRCCS and conformed to the ethical guidelines of the Declaration of Helsinki (1975).Written informed consent has been obtained from patients undergoing posterior mitral valve repair (MVR) and also from control subjects. We enrolled patients candidates for MVR due to posterior or anterior mitral valve prolapse (MVP) with severe regurgitation. Blood samples were obtained the day before surgery and mitral valve specimens were collected in saline solution immediately after mitral valve resection.

The preoperative inclusion criteria taken into consideration were: need for elective, isolated surgical procedure; patients over 18 year of age, an ejection fraction of > 30%, a normal sinus rhythm and no history of atrial fibrillation. Patients with bicuspid aortic valve, premature menopause and/or osteoporosis, previous aortic or mitral valve surgery, rheumatic heart disease, endocarditis, active malignancy, chronic liver failure, calcium regulation disorders (hyperparathyroidism, hyperthyroidism, and hypothyroidism), and chronic or acute inflammatory states (sepsis, autoimmune disease, and inflammatory bowel disease) were excluded.

Control subjects has been screened from those attending the Clinic for Global control of Cardiovascular Risk at Centro Cardiologico Monzino, IRCCS. The inclusion criteria were: over 18 years of age, normal sinus rhythm, no electrocardiographic alterations, no history of atrial fibrillation, cardiovascular risk factors similar to that of MVP patients but without cardiovascular diseases. In collaboration with the University of Pennsylvania, three healthy mitral valve leaflets were obtained from the Penn Cardiac Bio-registry.

3.2 Blood Sampling

Peripheral blood samples were drawn from the antecubital vein of patients (before surgery) and control subjects (on fasting stomach), using 2 tubes containing EDTA (9.3 mM; Vacutainer Systems, Becton Dickinson, Franklin Lakes, NJ, USA).

The first Vacutainer, containing whole blood, was kept on ice all the time. An aliquot was combined (1:1) with 10% trichloroacetic acid (TCA - Sigma-Aldrich, St Louis, MO, USA) and 1 mM EDTA and then soted at -80°C until oxidative stress measurements.

The second tube was used for plasma isolation. The tube was centrifuged at 3000 x g for 10 min at 4°C (within 30 min after being drawn) and the resulting plasma was aliquoted and stored at -80°C.

3.3 Endothelial and Interstitial Cell Isolation

Isolation of both mitral endothelial (VEC) and interstitial cells (VIC) was performed using a method described by *Poggio et al*. [94]. Briefly, mitral leaflets were placed in 2 mg/mL type II collagenase (Worthington Biochemical Corp., NJ, USA) in Advanced Dulbecco's modified Eagle's medium (DMEM – Thermo Scientific, MA, USA) containing 10% foetal bovine serum (FBS - Thermo Scientific, MA, USA) 1% Penicillin (Thermo Scientific, MA, USA), 1% Streptomycin solution (Thermo Scientific, MA, USA) and incubated for 20 min at 37°C. Loosened endothelial layer was removed by wiping the leaflet surfaces with sterile cotton swabs. The resulting cells were washed and isolated using Dynabeads® conjugated with platelet endothelial cell adhesion molecule (CD31 – Thermo Scientific, MA, USA), an endothelial marker, and cultured in M200 media supplemented with low serum growth supplement (LSGS - Thermo Scientific, MA, USA) on 0.1% gelatine (Sigma-Aldrich, St Louis, MO, USA) coated tissue culture plate. Afterwards, tissues were finely minced and dissociated

with type II collagenase (2 mg/mL) overnight at 37°C. The resulting VICs were seeded in tissue culture plates in supplemented advanced DMEM media. All the experiments were performed on cultured cells between their second and fifth passages. Cells were left untreated or treated with 10 mM β-glycerophosphate and 50 mg/mL ascorbic acid (βGAA - Sigma-Aldrich, St Louis, MO, USA) for 6 and 12 days or with 50 ng/mL osteoprotegerin (OPG - Prospecbio, USA) for 6 and 12 days unless specified elsewhere. β -glycerophosphate and ascorbic acid are able to induce *in vitro* endothelial mesenchymal transition [44].

3.4 RNA Extraction

RNA was extracted from VECs and VICs using the Total RNA Purification Plus Kit (Norgen Biotek Corp., Canada). Briefly, the cell monolayer was washed with phosphate-buffered solution (PBS – Euroclone, Milan, Italy) and then were lysed using a specific buffer provided in the kit. Following this, genomic DNA was removed and total RNA was purified using provided columns. RNA was quantified with Nanodrop (TECAN pro infinite M200) and used for two steps PCR amplification with TaqMan Reverse Transcription Reagent kit (Thermo Scientific, MA, USA). Total RNA (1 mg) was converted into complementary DNA (cDNA).

3.5 Real-Time and Digital PCR

Real Time PCR (qPCR) was performed on ABI Prism 7900 HT (Applied Biosystems), according to the manufacturer's instructions, to evaluate the relative expression of specific genes. The analysis was conducted with software SDS2.4 (Thermo Scientific, MA, USA) and gene expression levels were normalized with glyceraldehyde 3-phosphate dehydrogenase (GAPDH).

Digital PCR (dPCR) was carried out on a QuantStudio™ 3D Digital PCR System platform made up of the QuantStudio™ 3D Instrument, the Dual Flat Block GeneAmp® PCR System 9700 and the QuantStudio™ 3D Digital PCR Chip Loader (Thermo Scientific, MA, USA). dPCR manufacturer's instructions were followed and analysis was performed using QuantStudio® 3D AnalysisSuite™ (Thermo Scientific, MA, USA). Primers labelled with FAM® or VIC® dyes were used to evaluate the expression of targeted genes and the housekeeping gene respectively. Gene expression levels were normalized with ribosomal protein large P0 (RPLP0). The primers used are listed in **Appendix A**, **Table A1**.

3.6 Immunofluorescence

Immunofluorescence staining was performed to evaluate cell protein expression using specific antibodies against the platelet endothelial cell adhesion molecule (CD31 - Santa Cruz Biotechnology, Dallas, USA), α-smooth muscle actin (SMA- Abcam, Cambridge, United Kingdom) and vimentin (VIM - Cell Signaling Technology, Danvers ,USA). VICs and VECs were cultured in special immunofluorescence chambers (IBIDI GmbH, German) and fixed with paraformaldehyde (PFA - Sigma-Aldrich, St Louis, MO, USA) 4% for 15 minutes at room temperature. Cells were subsequently permeabilized with cold methanol for 10 minutes at room temperature and then incubated with blocking solution for 1 hour at room temperature. After washing, cells were incubated with the appropriate primary antibody overnight at 4°C protected from light. Cells were then washed with cold PBS and incubated with the secondary antibody for 2 hours at room temperature and protected from light. After washing, Vectashield mounting media with DAPI (Vector Laboratories, CA, USA) was added in order to detect cell nuclei. Zeiss Apotome microscope was used to capture the images.

3.7 Western blot

Western Blot analysis was carried out to assess protein expression using specific antibodies against phosphorylated syndecan 4 (pSDC4 - Santa Cruz Biotechnology, Dallas, USA - observed band molecular weight (MW) 24 kDa), SDC4 (Santa Cruz Biotechnology, Dallas, USA - observed band MW 24 kDa), Heparinase I (Hep I - Sigma-Aldrich, St Louis, MO, USA), phosphorylated extracellular signal-regulated kinase (pERK - Cell Signaling Technology - observed band MW 42/44 kDa), ERK (Santa Cruz Biotechnology, Dallas, USA - observed band MW 44 kDa), metalloproteinase 9 (MMP9 - Santa Cruz Biotechnology, Inc - observed band MW 89/92 kDa), osteoprotegerin (OPG - R&D Systems, Inc., Canada, USA), transforming growth factor beta 1 (TGFβ-1 - Cell Signaling Technology, Danvers, USA) and GAPDH (Cell Signaling Technology, Danvers, USA - observed band MW 37 kDa).

Briefly, after the treatments with or without TGβ1, OPG and Hep I, cells were collected and lysed in cell lysis buffer supplemented with a protease and or phosphatase inhibitor cocktail (Thermo Scientific, MA, USA). Total protein concentration was quantified with BCA kit (Thermo Scientific, MA, USA). Afterwards, proteins were separated on Bolt™ 4-12% Bis-Tris Plus Gels (Thermo Scientific, MA, USA) transferred onto nitrocellulose membrane and blocked with skim milk (Sigma-Aldrich, St Louis, MO, USA). Target proteins were detected by membrane incubation overnight at 4 °C with specific primary antibodies. Then the membranes were washed and incubated with peroxidase-conjugated secondary antibodies for another 2 h. Finally, the membrane was washed to remove any excess secondary antibody and incubated with Pierce™ ECL Western Blotting Substrate (Thermo Scientific, MA, USA) to detect specific bands. The images were acquired with the Alliance Mini 2M (UVITEC, Cambridge), and densitometric analysis of membranes was performed using the software ImageJ (Version 1.48m – National Institute of Health).

3.8 Collagen Assay

The Sircol Soluble Collagen Assay (Biocolor, United Kingdom) is a quantitative dye-binding method that has been designed for the analysis of soluble collagens released into cell culture medium during cell growth and/or specific cell treatments. In accordance with the manufacturer's instructions, we quantified total soluble collagen in cell culture supernatants after OPG treatment. Briefly, VECs or VICs were incubated in serum free DMEM with or without OPG for different time points (24 and 48 hours). At the end of treatment, the cell culture supernatants were collected and incubated with Sircol Dye Reagent in order to permit collagen-dye complex formation. Then unbound dye was removed from the surface of the complex using ice-cold Acid-Salt Wash Reagent. Finally, all the bound dye was dissolved with Alkali Reagent. The samples were read at 555nm and the results were expressed as a ratio between collagen concentration/ total protein (ng/ug).

3.9 Zymography

MMP9 activity was detected by gelatin zymography using cell culture supernatant collected after OPG treatment, following manufacturer’s instructions. Briefly, samples are run on Novex® Zymogram Gelatin Gel (Thermo Scientific, MA, USA) under non reducing conditions. After electrophoresis, the gel was renatured with Zymogram Renaturing Buffer and then incubated with Zymogram Developing Buffer. The gel was stained with Coomassie brilliant blue G-250 (Sigma-Aldrich, St Louis, MO, USA) and destained in water in order to identify regions of protease activity that appear as clear bands on a dark blue background where the protease has digested the substrate.

3.10 Flow Cytometry Analysis

Flow cytometry analysis was performed on 1% PFA fixed cells. For intracellular staining, cells were permeabilized with cold methanol for 30 minutes at 4°C followed by incubation with specific antibody tetramethylrhodamine isothiocyanante (TRITC)-conjugated. A total of 10,000 events per sample were acquired on a BD FACS Calibur. Cytometer performances were checked by daily running BD Cytometer Setup and Tracking Beads. Data were reported as mean fluorescence intensities (arbitrary units), calculated from fluorescence histograms for population or as percentage of cells positive for the analysed antigens. All the data were analysed with FlowJo vX.0.7 Software.

3.11 Migration Assay

The directional cell migration assay was performed using 24-well plate with culture inserts (IBIDI GmbH, German). Briefly, VECs and VICs were seeded in the inserts of the 24-well system and allowed to adhere overnight. Inserts were removed to create a cell-free gap of approximately 500 μm, and cells were allowed to migrate for 24 hours at 37°C and 5% CO_2 in the presence of OPG or in the medium alone. Every 3 hours pictures of the gaps were taken with the ZEISS ApoTome and ImageJ (Version 1.48m – National Institute of Health) was used to analyse the cell free area.

3.12 Osteoprotegerin Quantification

Blood was collected form patients and control subjects and processed to obtain plasma. OPG plasma levels were evaluated by enzyme-linked immunosorbent assay (ELISA - R&D Systems, Inc., Canada, USA) in accordance with the manufacturer's instructions.

3.13 Oxidative Stress Measurements

The oxidative stress evaluation was assessed by a previously developed and validated LC-MS/MS method [95]. The ratio between oxidized (GSSG) and reduced (GSH) form of glutathione (GSSG/GSH) is a well-recognized index. GSSG and GSH levels were measured on whole blood with added 10% TCA in 1 mM EDTA solution to precipitate proteins.

3.14 Proliferation Assay

Cells were seeded in 96 well plate and the day after were incubated with or without OPG for 24 hours. At the end of the treatments, the medium was removed and the 3-(4, 5-dimethylthiazolyl-2)-2,5-diphenyltetrazolium bromide (MTT - Sigma-Aldrich, St Louis, MO, USA) solution (0.5 mg/ml) was added into each wells and incubated at 37°C, 5% CO_2 for 2 hours. Then the supernatant was discarded and dimethylsulfoxide (DMSO - Sigma-Aldrich, St Louis, MO, USA) was added into each wells. The corresponding absorbance value was observed using the microplate reader (TECAN pro infinite M200) at dual wavelength of 590 nm and 620 nm.

3.15 Statistical Analysis

Data were analysed using IBM SPSS statistic software (version 22) and Graph Pad Prism software (version 6). Continuous variables were expressed as mean ± standard error (SEM). For comparisons of continuous and categorical data, the parametric T-test and the Pearson Chi-square test were used respectively.

3.15.1 Binary logistic regression model

Continuous variables are summarized as mean ± SE, except for age, which is represented as mean [minimum, maximum], while categorical variables are summarized as frequency and percentage.

For data analysis, the Mann-Whitney test was performed between MVP and control classes on continuous variables, while Fisher's exact test on discrete ones.

Finally, taking into account the OPG measurement and GSSG/GSH ratio together with body mass index (BMI), several logistic regression procedures were implemented in order to identify a classification rule, capable of predicting outcomes with the highest accuracy.

The logistic model is:

$$p(Y_i = 'MVP') = \frac{1}{1 + e^{-(\beta_0 + \beta_1 x_1 + \beta_2 x_2 + \beta_3 x_3)}}$$

Where, p = probability to have MVP, x_1 = OPG measurement (in pg/mL), x_2 = GSSG/GSH ratio and x_3 = BMI (Kg/m^2).

A receiver operating characteristic (ROC) curve was plotted for each model and performances were evaluated by comparing areas under the ROC Curve (AUC).

4. *IN VITRO* STUDY

The data reported in the following chapter have been published as:

Songia P *et al.* ***Mitral valve endothelial cells secrete osteoprotegerin during endothelial mesenchymal transition***. Journal of Molecular and Cellular Cardiology. 23;98:48-57; 2016.

4.1 Human mitral valve endothelial and interstitial cell characterization

We enrolled and collected specimens from twenty-five patients affected by posterior mitral valve prolapse (MVP) who underwent surgical repair. From the collected specimens, we isolated endothelial (VECs) and interstitial cells (VICs). At phase contrast microscopy, VECs showed classical cobblestone morphology, while VICs a spindle shape one (**Figure 4.1A**). In addition, immunofluorescence staining revealed that VECs were positive for platelet endothelial cell adhesion molecule (CD31) at the cell-cell borders, vimentin (VIM) throughout the cytoplasm but not for α-smooth muscle actin (SMA) (**Figure 4.1A**). In contrast, VICs were positive for SMA, VIM and negative for CD31 (**Figure 4.1B**).

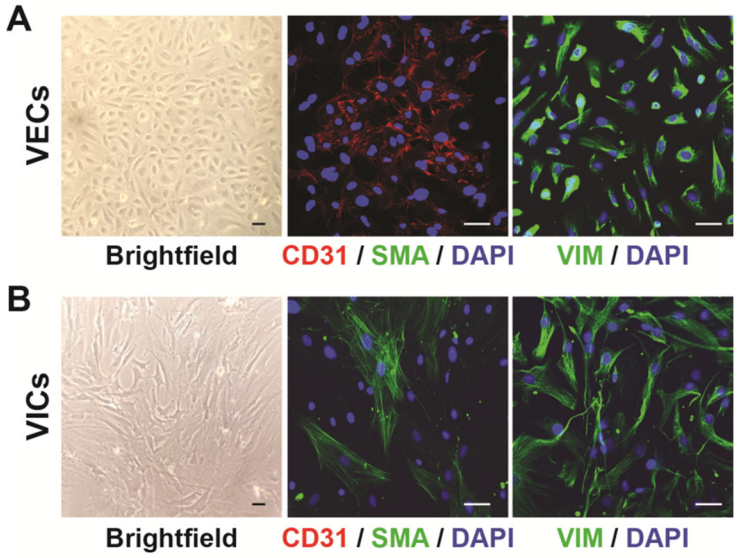

Figure 4.1 Human mitral valve endothelial and interstitial cell characterization. (**A-B**) Phase contrast imaging and immunofluorescence staining for platelet endothelial cell adhesion molecule (CD31 – Red), smooth muscle actin (SMA – Green), vimentin (VIM – Green) and 4',6-diamidino-2-phenylindole (DAPI, for nuclei detection – Blue), in human isolated valve endothelial (VEC) and interstitial cells (VIC) from mitral valve prolapse patients. Scale bar, 20 μm.

4.2 Human mitral valve endothelial cells undergo endothelial to mesenchymal transition

Cells were treated for 6 and 12 days with β-glycerophosphate and ascorbic acid (βGAA) to induce endothelial mesenchymal transition (EndMT). We performed a quantitative PCR (qPCR), flow cytometric and morphological analysis to confirm that EndMT occurred after βGAA treatment (**Figure 4.2**). In particular, we observed a significant ($p<0.05$) upregulation of SMA and collagen III (Col3A1) RNA levels after 6 days of treatment (4.5±0.9 and 3.0±0.6 fold, respectively) (**Figure 4.2A**). Furthermore, after 12 days of βGAA treatment, RNA analysis showed a significant ($p<0.05$) upregulation of bone morphogenetic protein 4 (BMP4) and collagen I (Col1A1) by 3.0±0.7 and 10.8±3.2 fold, respectively (**Figure 4.2B**). We also performed a flow cytometric analysis that underlined an overexpression of SMA on VECs treated with βGAA (**Figure 4.2C**). Finally, we observed VECs morphological changes from cobblestone to spindle-shape (**Figure 4.2D**). All these results confirmed that during βGAA treatment the isolated VECs underwent EndMT.

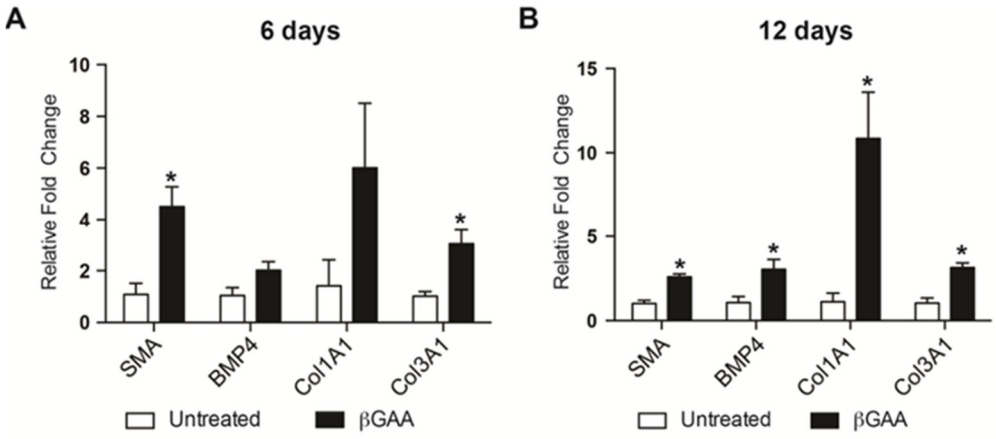

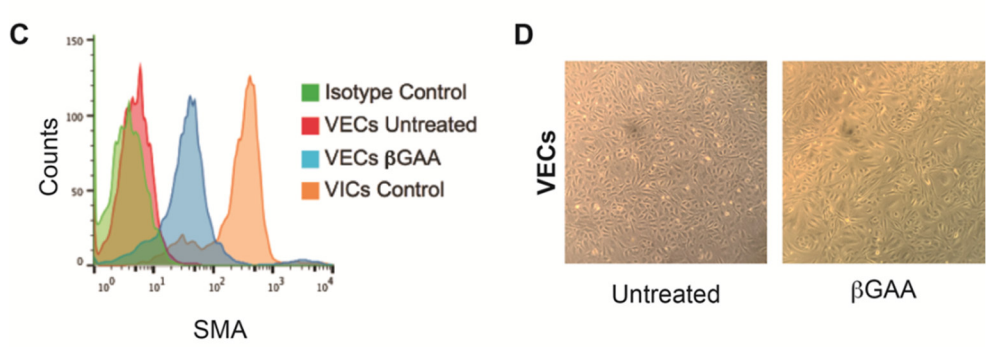

Figure 4.2 Endothelial to mesenchymal transition of human mitral valve endothelial cells. (**A-B**) Quantitative PCR (qPCR) of smooth muscle actin (SMA), bone morphogenetic protein 4 (BMP4), collagen I (Col1A1) and collagen III (Col3A1) of valve endothelial cells (VEC) in absence or in presence of β-glycerophosphate and ascorbic acid (βGAA) for 6 or 12 days (n = 3). (**C**) Flow cytometric analysis (FACS) of SMA for isotype control, untreated VEC, VEC treated with βGAA for 6 days and activated valve interstitial cells (VIC) as a positive control (n=3). (**D**) Phase contrast imaging of untreated VECs or treated for 12 days with βGAA. Magnification: 20X. * $p<0.05$.

4.3 Endothelial to mesenchymal transition induces osteoprotegerin expression and secretion

We analysed the expression of OPG in prolapsed (n = 3) and healthy mitral valve leaflets (n = 3). The Western blot analysis, carried out on whole tissue extract, underlined a significant ($p<0.05$) increase in prolapsed leaflets in comparison to healthy ones (**Figure 4.3A and B**). To understand better the OPG role in the MVP progression, we evaluated if VECs expressed and/or secreted OPG during EndMT. The experiments forcing VECs to undergo EndMT highlighted a significant ($p<0.05$) increased expression of OPG RNA levels at 6 and 12 days (1.9±0.4 and 4.1±1.3 fold, respectively) (**Figure 4.3C**). In addition, implementing a commercially available ELISA, we observed that VECs secreted more OPG in comparison to untreated cells during the first 6 days of βGAA treatment (2369±564.7 pg/µg of total protein *vs.* 923.5±261.1 pg/µg of total protein, respectively; $p<0.05$ – **Figure 4.3D**).

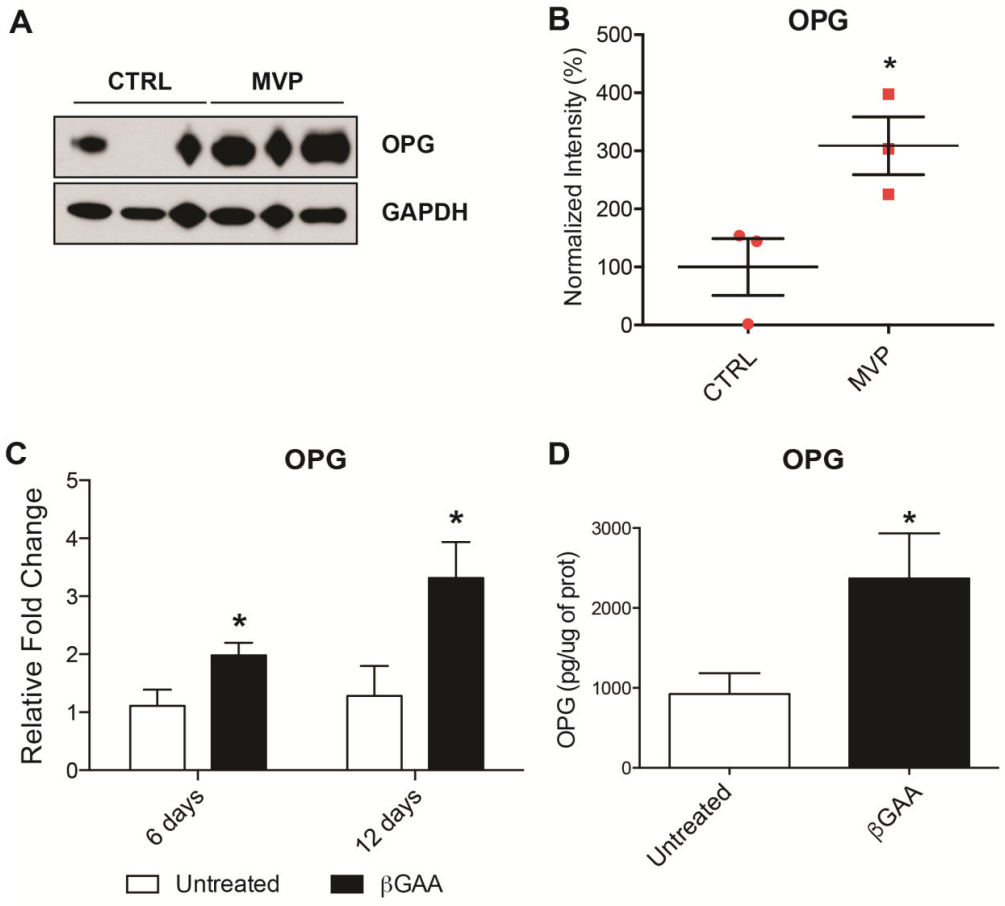

Figure 4.3 Endothelial to mesenchymal transition induces osteoprotegerin expression and secretion. (**A**) Western blot of osteoprotegerin (OPG) and glyceraldehyde 3-phosphate dehydrogenase (GAPDH), as endogenous control, of mitral valve prolapse (MVP) patients and controls subjects (CTRL). (**B**) Western blot quantification using ImageJ (n=3). * $p<0.05$. (**C**) Quantitative PCR (qPCR) of osteoprotegerin (OPG) of valve endothelial cells (VEC) in absence or in presence of β-glycerophosphate and ascorbic acid (βGAA) for 6 or 12 days (n = 3). (**D**) OPG enzyme-linked immunosorbent assay (ELISA) on media of untreated and βGAA treated VEC for 6 days (n=3). * $p<0.05$.

4.4 Osteoprotegerin interacts with syndecan family receptors in endothelial cells

To understand better the possible directed OPG effects on endothelial cells, the first step was to evaluate if VECs expressed a specific receptor(s) capable of interacting with OPG and triggering protein expression already known to be involved in MVP. Accordingly, we carried out digital PCR (dPCR) analyses on nine different VEC preparations and we observed that this particular cell type expressed all syndecan receptors at different levels (SDC1, SDC2, SDC3 and SCD4). As shown in **Figure 4.4** the expression levels were: SDC1 2.07±0.62% with a precision of 2.97%; SDC2 0.41±0.05% with a precision of 5.49%; SDC3 2.42±0.50% with a precision of 3.50%; SDC4 1.03±0.23 with a precision of 4.85%. All the data used for the relative quantification are listed in **Appendix A**, **Table A2**.

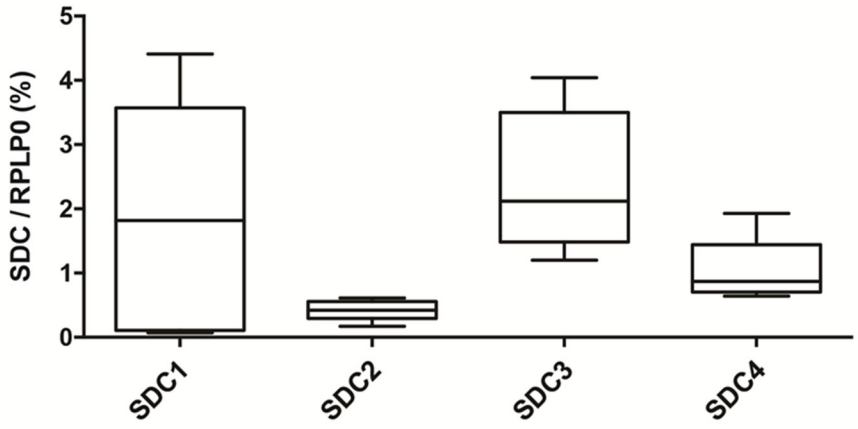

Figure 4.4 Syndecan expression in endothelial cells. Digital PCR (dPCR) analysis of the syndecan family (SDC1, 2, 3 and 4) on nine different valve endothelial cell populations. Ribosomal protein large P0 (RPLP0) was used as housekeeping gene.

To prove OPG-SDC interaction, we analysed SDC4 phosphorylation (serine 179 - pSDC4) upon OPG treatment. This residue is highly conserved among the family [96] and once it is phosphorylated the signalling cascade is shutdown [97]. We performed a Western blot analysis and we observed a decrement in pSDC4 at 5 and 15 minutes after OPG treatment (**Figure 4.5A**). To confirm these results, we pre-treated VECs with Heparinase I (Hep I). Hep I is able to inactivate the syndecans by removing the heparan sulphate domain presents in the extracellular portion of these receptors. As reported in **Figure 4.5B,** we observed the completed inhibition of SDC4 dephosphorilation after Hep I pre-treatment. (**Figure 4.5B**). The apparent loss of SDC4 could be due to protein destabilization after Hep I pre-treatment or the specific antibody used may require heparan sulphate domain to completely bind SDC4.

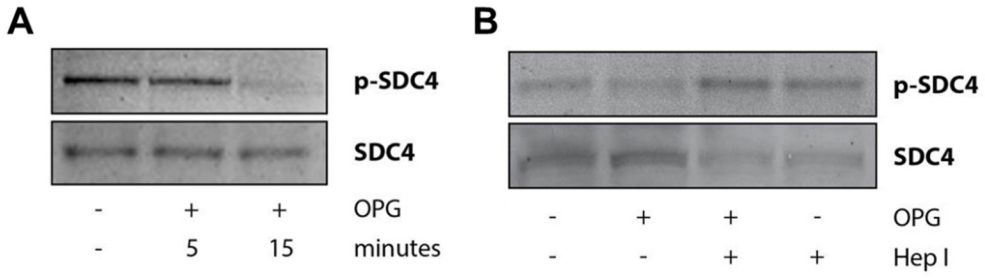

Figure 4.5 Osteoprotegerin and Syndecan 4 in human mitral valve endothelial cells. (**A**) Western blot of phosphorylated syndecan 4 (pSDC4) and syndecan 4 (SDC4) in valve endothelial cells (VECs) after osteoprotegerin (OPG) treatment for 5 and 15 minutes. (n = 3). (**B**) Western blot of pSDC4, SDC4, in absence or presence of OPG or Heparinase I (Hep I) pre-treatment (5 U/ml) and OPG (n = 3).

To characterize OPG signalling cascade in MVP, we evaluated extracellular signal-regulated kinase 1 and 2 (ERK). Indeed, ERK phosphorylation upon OPG treatment has already been shown in chondrocytes and in endothelial cells [98, 99]. OPG successfully induced ERK activation and Hep I pre-treatment completely blocked this effect (**Figure 4.6A**). In addition, to verify the specificity of Hep I on SDCs we treated VECs with transforming growth factor

beta 1 (TGFβ-1), a recognized ERK activator, in the presence or absence of Hep I. As reported in **Figure 4.6B**, we observed that Hep I pre-treatment was not able to prevent the ERK activation induced by TGFβ-1 (**Figure 4.6B**).

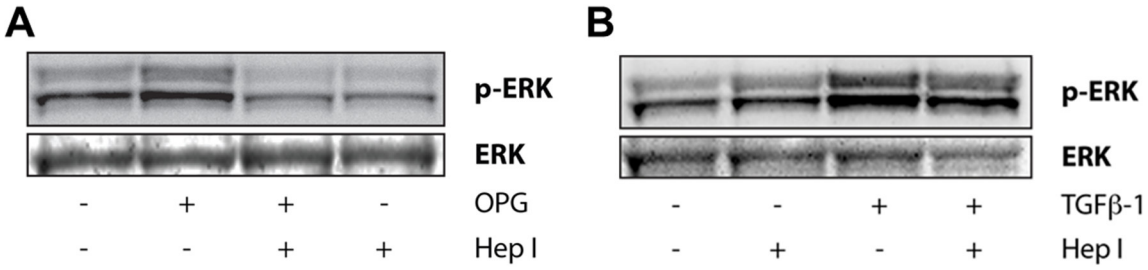

Figure 4.6 Osteoprotegerin, extracellular signal-regulated kinase activation and Heparinase I specificity in human mitral valve endothelial cells. (**A**) Western blot of phosphorylated extracellular signal-regulated kinase (pERK) and ERK, in absence or presence of ostoeprotegerin (OPG) or Heparinase I (Hep I) pre-treatment (5 U/ml) and OPG (n = 3). (**B**) Western blot of pERK and ERK, in absence or presence of transforming growth factor beta 1 (TGFβ-1 - 5 ng/mL) or Hep I pre-treatment and OPG.

All these results enable us to confirm that OPG interact with syndecan receptors and that Hep I is specific for these receptors.

4.5 Osteoprotegerin induces extracellular matrix changes in endothelial cells

Since isolated VECs express and activate syndecan receptors, we could investigate possible effects of OPG on endothelial cells. First, we checked the expression of known OPG downstream partners, such as integrin alpha V and beta 3 [98]. We performed a qPCR analysis and observed a significant ($p<0.05$) increase of both integrins after OPG treatments (4.4±0.9 and 20.9±7.5, respectively; - **Figure 4.7**).

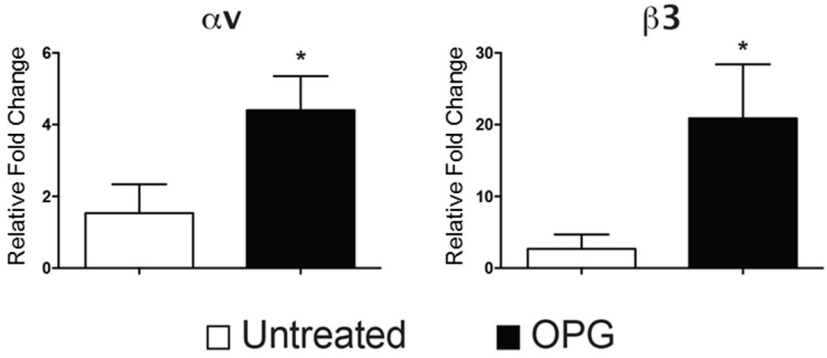

Figure 4.7 Osteoprotegerin and integrin expression in endothelial cells. Quantitative PCR (qPCR) of integrins alpha 5 (αv) and beta 3 (β3) of valve endothelial cells (VEC) untreated or treated for 12 days with 50 ng/ml of osteoprotegerin (OPG) (n=5). * $p<0.05$.

Secondly, we evaluated several proteins such as collagens, BMP4, proteoglycans and metalloproteinases (MMPs) that are known to be regulated in MVP [30, 33, 93]. We identified a significant increase of Col1A1 (+4.0±0.6; $p<0.001$), Col3A1 (+3.0±0.6; $p<0.01$) (**Figure 4.8A**), BMP4 (+2.4±0.7; $p<0.05$) and versican (VCAN), an extracellular matrix proteoglycan (+3.8±0.2; $p<0.001$) (**Figure 4.8B**).

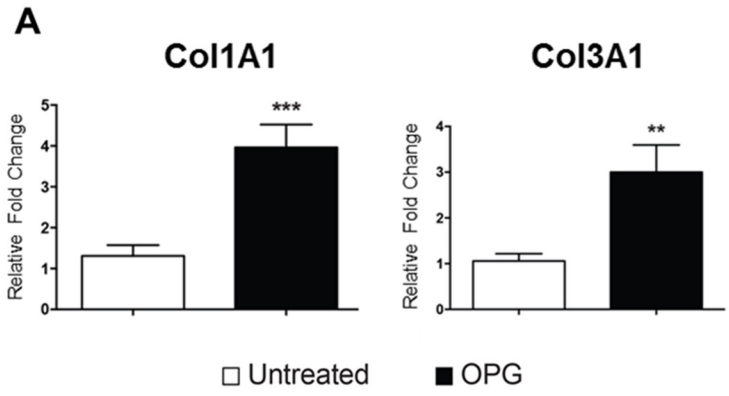

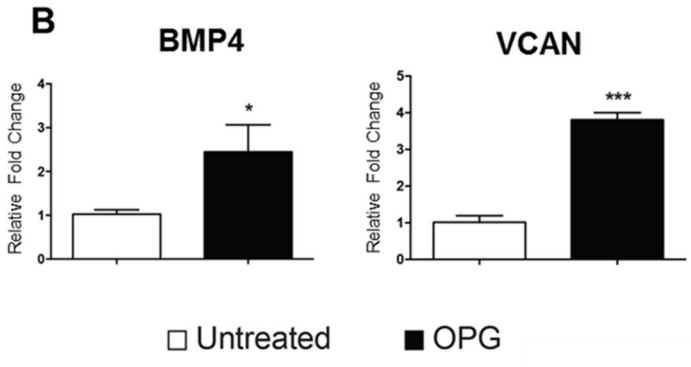

Figure 4.8 Osteoprotegerin and extracellular matrix changes in endothelial cells. (**A**) Quantitative PCR (qPCR) of collagen I (Col1A1), collagen III (Col3A1), (**B**) bone morphogenetic protein 4 (BMP4) and versican (VCAN) of valve endothelial cells (VEC) untreated or treated for 12 days with 50 ng/ml of osteoprotegerin (OPG) (n=5). * $p<0.05$; ** $p<0.001$; *** $p<0.0001$.

To further confirm OPG effects on VECs, we evaluated total collagen production by colorimetric assay. We treated the endothelial cells for 48 hours in either the presence or the absence of OPG and we observed that treated cells secreted more collagen compared to untreated cells (13.4±0.7 *vs.* 11.3±0.4 ng of collagen / µg of total protein, respectively; $p<0.05$) (**Figure 4.9A**). Beside protein levels, it has been shown that MMPs activity may play an important role in the progression of the disease [30, 93]. We found higher MMP9 expression and activity after OPG treatment (**Figure 4.9B and C**).

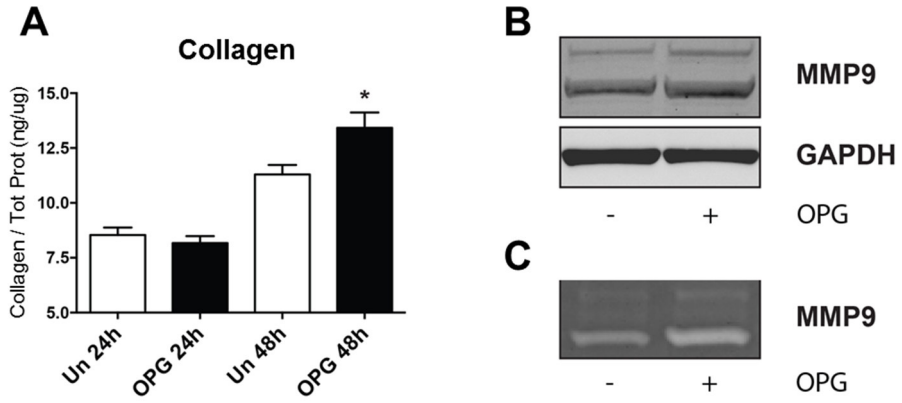

Figure 4.9 Osteoprotegerin effects on endothelial cells. (**A**) Total soluble collagen produced by untreated or osteoprotegerin (OPG - 50 ng/ml) treated VECs for 24 and 48 hours (n = 5); * $p<0.05$. (**B**) Western blot and (**C**) gelatin zymography gel of matrix metalloproteinase 9 (MMP9) in VECs untreated or treated with OPG (50 ng/ml) (n = 3). Glyceraldehyde 3-phosphate dehydrogenase (GAPDH), as endogenous control.

4.6 Osteoprotegerin induces endothelial to mesenchymal transition

To further characterize OPG effects on VECs, we investigated if OPG could drive EndMT. Along with increased expression of SMA and fibroblastic specific protein 1 (FSP1) markers, endothelial cells undergoing EndMT acquire migratory properties [14]. We observed a significant ($p<0.05$) increase of SMA (+1.6±0.2) and FSP1 (+1.9±0.3) after OPG treatments (**Figure 4.10**).

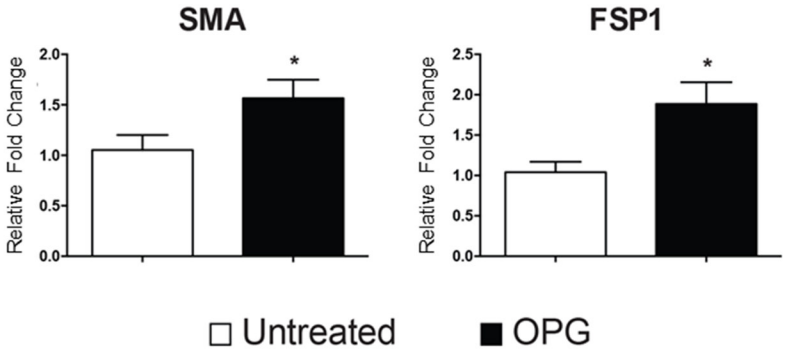

Figure 4.10 Osteoprotegerin induces endothelial to mesenchymal transition. Quantitative PCR (qPCR) of smooth muscle actin (SMA) and fibroblast specific protein 1 (FSP1) of valve endothelial cells (VEC) untreated or treated for 12 days with 50 ng/ml of osteoprotegerin (OPG) (n=5). * $p<0.05$.

In addition, evaluating the percentage of the closed area in a migration assay, we showed that VECs under OPG stimuli (24 hours) were able to migrate faster that untreated cells (area closed 43.3±3.9% and 21.8±2.6% untreated cells; $p<0.001$ - **Figure 4.11A and B**). Interestingly, already after 6 hours, the VECs were able to migrate faster than controls ($p<0.05$ – **Figure 4.11A and B**).

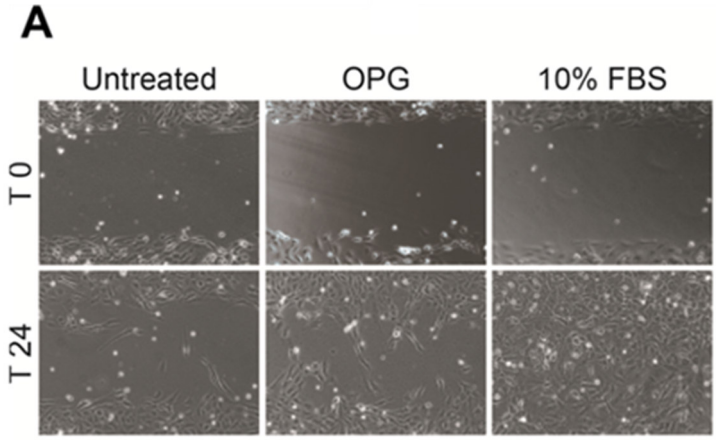

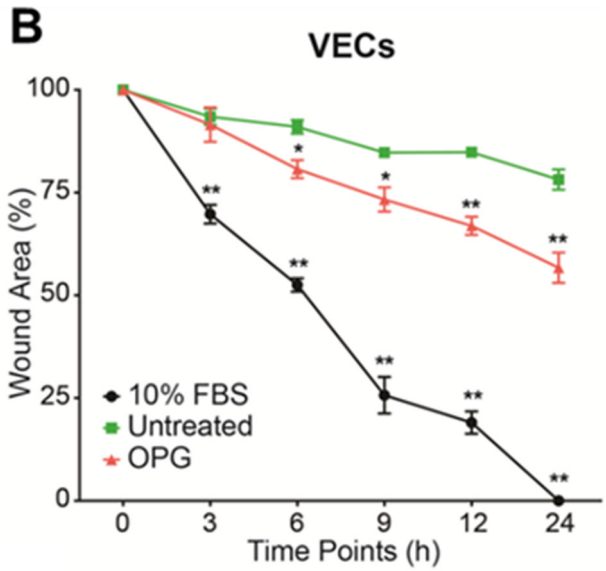

Figure 4.11 Osteoprotegerin induces cell migration in endothelial cells. (**A**) Representative images of wound healing assay for VECs in presence of OPG (50 ng/mL) or 10 % foetal bovine serum (FBS - positive control). (**B**) Time course representing the percentage of the area without migrating VECs in presence of OPG (50 ng/mL) or 10 % FBS (n = 5). * $p<0.05$; ** $p<0.01$.

Furthermore, to verify whether OPG-induced VEC migration was caused by OPG-SDC interaction, we carried out the same migration assay in the presence of Hep I. The results confirmed that the VECs lost they migratory ability after Hep I pre-treatment. In particular, the percentage of the closed area of OPG + Hep I (26.5±3.6%) was significantly ($p = 0.001$) lower than cells treated only with OPG (43.0±3.1%) and no differences were noticed with the negative control (**Figure 4.12A and B**).

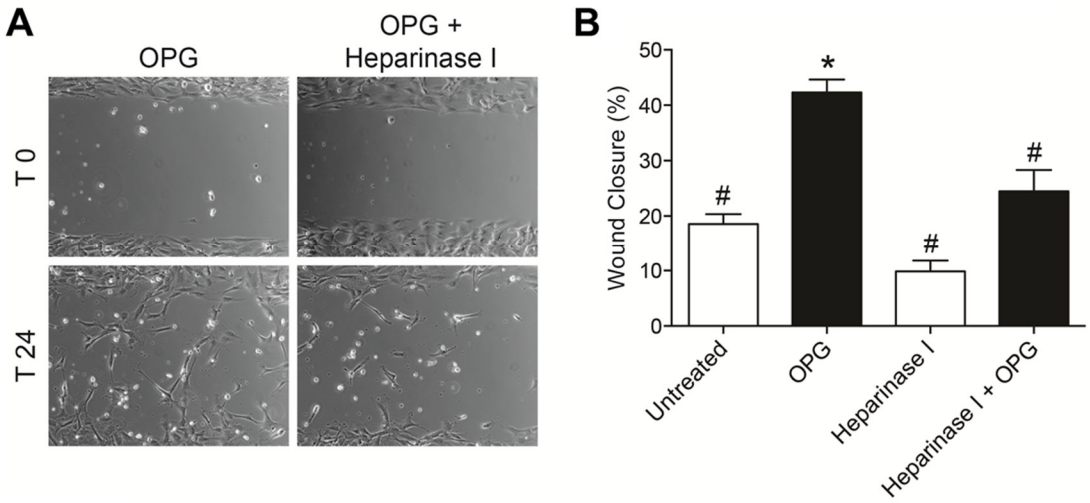

Figure 4.12 Osteoprotegerin, heparinase I and endothelial cell migration. (**A**) Representative images of wound healing assay for VECs in presence of OPG (50 ng/mL) with or without heparinase I pre-treatment (5 U/mL). (**B**) Bar graph depicting the percentage of migrating VECs in absence or presence of OPG (50 ng/ml) or heparinase I pre-treatment (5 U/mL) after 24 hours in presence of OPG (50 ng/mL) (n = 3). * $p<0.05$ vs. untreated; # $p<0.05$ vs. OPG treated VECs.

In conclusion, together, these results showed that endothelial cell migration induced by OPG occurred throughout the activation of the syndecan receptors.

4.7 Osteoprotegerin induces proliferation in interstitial cells and proteoglycan overexpression

Since interstitial cells represent another cells type involved in the mitral valve degeneration [33], we also evaluated the possible OPG effects on VICs. We implemented, as well as for VECs, dPCR technique and we observed that all syndecan receptors are expressed at different levels (**Figure 4.13**). In particular, the expression levels were: SDC1 0.64±0.34% with a precision of 11.74%; SDC2 11.43±1.53% with a precision of 2.56%; SDC3 7.31±1.28% with

a precision of 3.61%; and SDC4 4.08±1.04 with a precision of 3.80%. All the data used for the relative quantification are listed in **Appendix A, Table A3**.

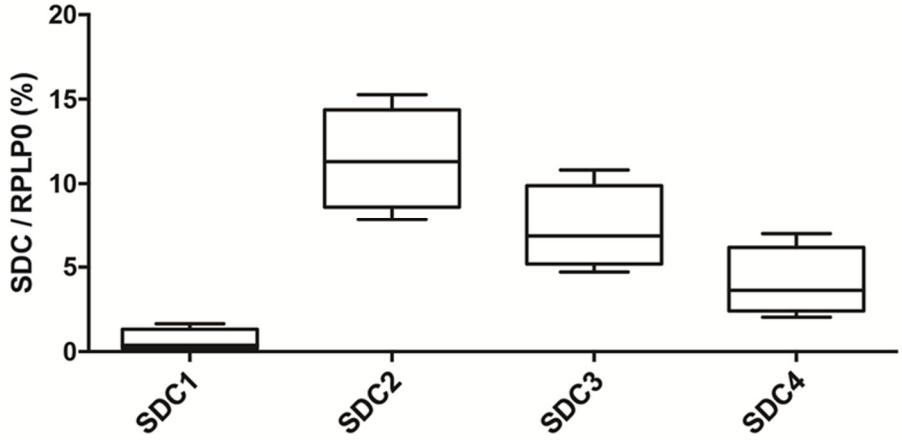

Figure 4.13 Syndecan expression in interstitial cells. Digital PCR (dPCR) analysis of the syndecan family (SDC1, 2, 3 and 4) on three different valve interstitial cell populations. Ribosomal protein large P0 (RPLP0) was used as housekeeping gene.

A previous study [100] showed that OPG was able to increase smooth muscle cell proliferation but there were no data about its possible effect on interstitial cells isolated from human mitral valves. To test whether OPG treatment for 24 hours could induce some effects on VIC proliferation, we performed a 3-(4,5-dimethylthiazol-2-yl)-2,5-diphenyltetrazolium bromide (MTT) assay. The results highlighted that OPG led to a significant increase of VICs proliferation (22.4% increment; p value < 0.05 – **Figure 4.14A**). In addition, we also evaluated if OPG could affect VIC migratory ability. In contrast to VECs, we did not notice any significant variation in VIC migration under OPG stimuli (**Figure 4.14B**).

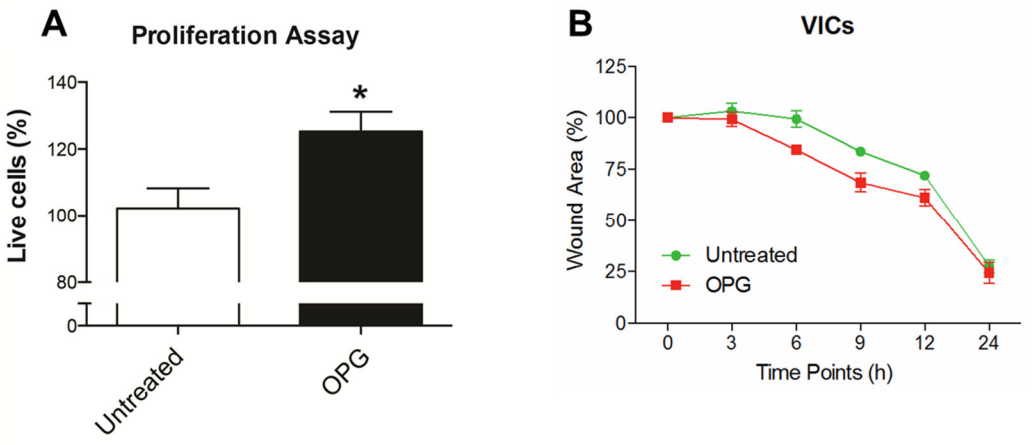

Figure 4.14 Osteoprotegerin on interstitial cell proliferation and migration. (**A**) Proliferation assay of valve interstitial cells (VIC) in absence or presence of osteoprotegerin (OPG - 50 ng/mL) for 6 days (n = 3) * $p<0.05$. (**B**) Time course representing the percentage of the area without migrating VICs in absence or presence of OPG (50 ng/ml).

Finally, we analysed the possible changes in RNA levels for the main proteins involved in the progression of mitral valve diseases [33, 81, 101]. VICs treated for 12 days with OPG showed a significant RNA level increment of BMP4 (+1.6±0.1; $p<0.05$), biglycan (BGN, +1.9±0.3; $p<0.001$), VCAN (+1.5±0.2; $p<0.05$), MMP2 (+1.6±0.1; $p<0.01$), SMA (+1.6±0.2; $p<0.05$), Col1A1 (+2.24±0.29; $p<0.001$) and Col3A1 (+1.58±0.29; $p<0.05$ - **Figure 4.15**). Interestingly, we noticed a significant upregulation of OPG (+1.5±0.2; $p<0.05$ – **Figure 4.15**).

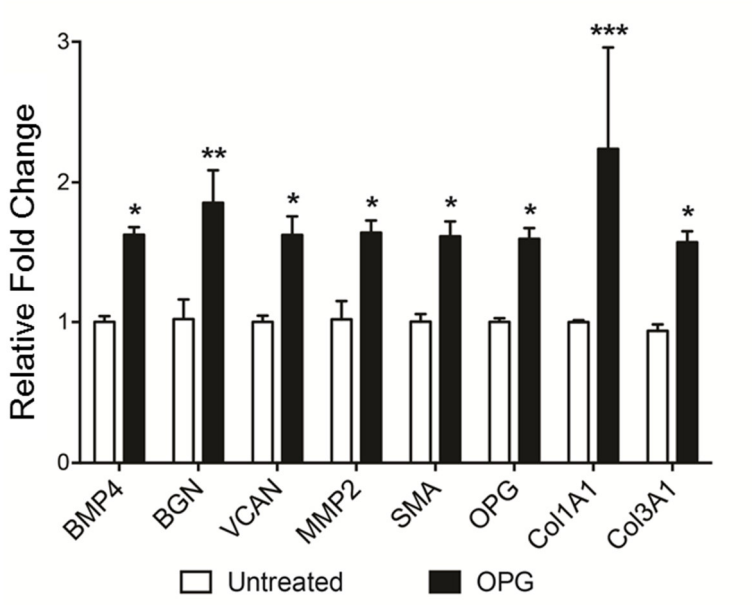

Figure 4.15 Osteoprotegerin induces proteoglycan expression in interstitial cells. Quantitative PCR (qPCR) of bone morphogenetic protein 4 (BMP4), biglycan (BGN), versican (VCAN), metalloproteinase 2 (MMP2), smooth muscle actin (SMA), osteoprotegerin (OPG), collagen I (Col1A1) and collagen III (Col3A1) of valve interstitial cells (VIC) untreated or OPG treated (50 ng/ml) for 6 days (n = 3). * $p<0.05$; ** $p<0.01$; ; *** $p<0.001$

To characterize better OPG effects on VICs, we also evaluated the total collagen production by colorimetric assay. After 48 hours of OPG treatment ,VICs showed a significant increase of collagen secretion in comparison to untreated cells (18.5±0.4 *vs.* 16.4±0.3 ng of collagen / µg of total protein, respectively; $p<0.05$) (**Figure 4.16**).

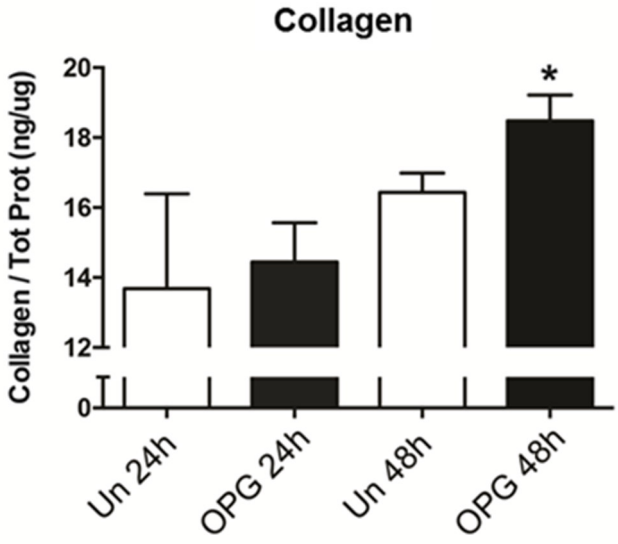

Figure 4.16 Osteoprotegerin and collagen production in interstitial cells. Total soluble collagen produced by untreated or osteoprotegerin (OPG - 50 ng/ml) treated valve interstitial cells (VIC) for 24 and 48 hours (n = 5); * $p<0.05$.

5. HUMAN STUDY

5.1 Osteoprotegerin plasma levels in MVP patients with severe regurgitation

Since OPG has direct effects on endothelial cells, we investigated OPG plasma levels in MVP patients. The analysis was carried out on 28 posterior MVP patients and 29 control subjects. The two groups had no statistically significant differences and the control subjects were selected with similar cardiovascular risk factors to MVP patients. In our population we observed, as previously reported [53], a positive correlation between OPG levels and age (**Figure 5.1A**).Therefore all the analysis was performed using a model adjusted for this variable. The main characteristics regarding all subjects are reported in **Table 5.1**.

Table 5.1 Demographic characteristics in controls and MVP patients

Variable	Control (N=29)	MVP (N=28)	p value
Age (years)	57.3 ± 11.1	60.8 ± 12.2	0.263
Male subjects	19 (65.5%)	19 (67.9%)	1.000
Diabetes	3 (10.3%)	3 (10.7%)	1.000
Hypertension	14 (48.3%)	11 (39.3%)	0.811
Hypercholesterolemia	14 (48.3%)	16 (57.1%)	0.822
Smokers	6 (20.7%)	3 (10.7%)	0.484

MVP: mitral valve prolapse. (percentage). Mean ± standard deviation

We identified a significant ($p<0.0001$) increase of OPG plasma levels in patients with posterior MVP in comparison to control subjects (1953±127.5 *vs.* 1109±45.3 pg/mL, respectively; **Figure 5.1B**).

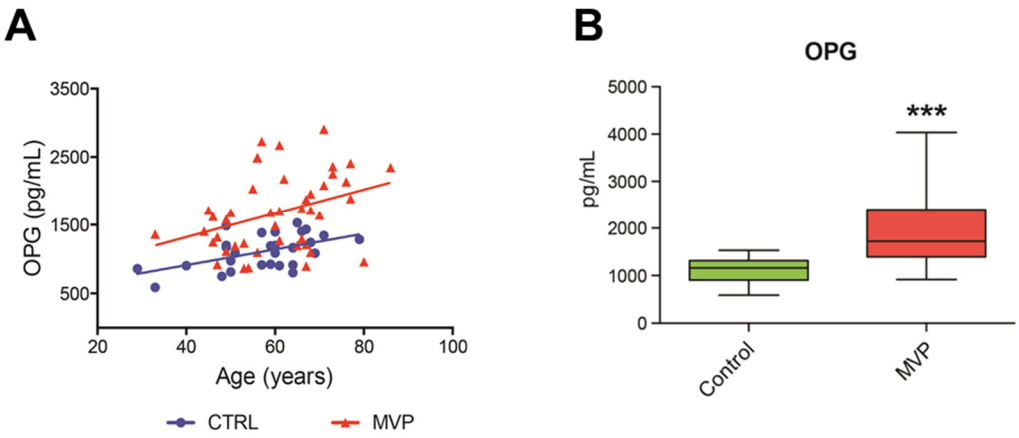

Figure 5.1 Osteoprotegerin plasma levels in patients with mitral valve prolapse. (**A**) Graph representing the correlation of osteoprotegerin (OPG) plasma levels with mitral valve prolapse (MVP) patients and control subjects (CTRL). (**B**) OPG enzyme-linked immunosorbent assay (ELISA) on plasma samples from control subjects or MVP patients. (Control subjects n = 29 and Mitral Valve Patients n = 28) *** $p<0.0001$.

5.2 Patient characteristics

Considering the previous results, we enrolled patients with either posterior MVP or anterior prolapse. The analysis was carried out on 43 MVP compared with 29 controls. Controls and patients were matched for age, sex, diabetes, hypertension, hypercholesterolemia and smoking. The two groups were comparable for all clinical and demographic features taken into consideretation, except for BMI and New York Heart Association (NYHA) class which were significantly lower ($p = 0.005$) and higher ($p<0.001$) in MVP patients than in controls (**Table 5.2**) respectively. All demographic characteristics and clinical details regarding the two populations are summarized in **Table 5.2**. In addition, the pharmacological treatments were not significantly different between MVP and controls, except for beta-blockers, mostly taken by patients (**Table 5.3**). However, up to now, there is no evidence of any influence of this class of

drugs on oxidative stress levels. In all patients, blood collection was performed before coronary angiography and surgery, while in control subjects during a scheduled visit.

Table 5.2 Clinical and demographic features in controls and MVP patients

Variable	Control (N=29)	MVP (N=43)	p Value
Age (years)	57.3 [53.2, 61.4]	60.1 [56.8, 63.5]	0.291
Sex (male)	19 (65.5%)	29 (67.4%)	0.865
Diabetes	3 (10.3%)	3 (7.0%)	0.685
Hypertension	14 (48.3%)	16 (37.2%)	0.660
Hypercholesterolemia	14 (48.3%)	25 (58.1%)	0.688
Smokers	6 (20.7%)	5 (11.6%)	0.514
BMI	27.4 ± 0.76	24.8 ± 0.43	**0.005**
Total Cholesterol (mg/dL)	216.1 ± 7.4	215.2 ± 6.6	0.973
Triglycerides (mg/dL)	111.2 ± 9.0	110.3 ± 6.7	0.690
HDL (mg/dL)	55.8 ± 3.2	51.3 ± 1.9	0.249
LDL (mg/dL)	138.0 ± 7.1	132.4 ± 6.5	0.658
LVEF (%)	65.9 ± 1.6	63.0 ± 1.6	0.4159
NYHA Class			**0.001**
I	29 (100%)	19 (44.2%)	
II	-	17 (39.5%)	
III	-	7 (16.3)	
IV	-	-	

BMI: body mass index; HDL: high-density lipoprotein; LDL: low-density lipoprotein; LVEF: left ventricular ejection fraction; MVP: mitral valve prolapse; NYHA: New York Heart Association. [minimum, maximum]; (percentage); mean ± standard error.

Table 5.3 Drug therapies in controls and MVP patients

Drug therapies	Control (N=29)	MVP (N=43)	p Value
Antiplatelets (%)	1 (3%)	2 (5%)	1.00
Angiotensin receptor blockers (%)	4 (14%)	3 (7%)	0.429
Converting enzyme inhibitors (%)	5 (17%)	14 (32%)	0.295
Calcium channel blockers (%)	3 (10%)	3 (7%)	0.679
Beta-blockers (%)	1 (3%)	16 (37%)	**0.007**
Nitrates (%)	0 (0%)	1 (2%)	1.00
Statins (%)	6 (21%)	6 (14%)	0.527

MVP: mitral valve prolapse; (percentage).

5.3 Osteoprotegerin levels and oxidative stress status

We evaluated OPG plasma levels and the analysis permitted us to confirm previous results (1748 ± 100.2 pg/mL in patients *vs.* 1109 ± 45.3 pg/mL in control subjects ($p<0.0001$- **Figure 5.2A**). In addition, the difference between the groups remain significant ($p<0.001$) also after age- and NYHA class- adjustment. Finally, we confirmed that the oxidative stress status, represented by GSSG/GSH ratio, was higher in MVP patients compared to control subjects (0.116 ± 0.007 vs. 0.053 ± 0.013, respectively; $p<0.0001$ – **Figure 5.2B**) and remained significant even after NYHA class adjustment ($p<0.001$). Notice that no correlation has been found between NYHA class and OPG levels or GSSG/GSH ratio.

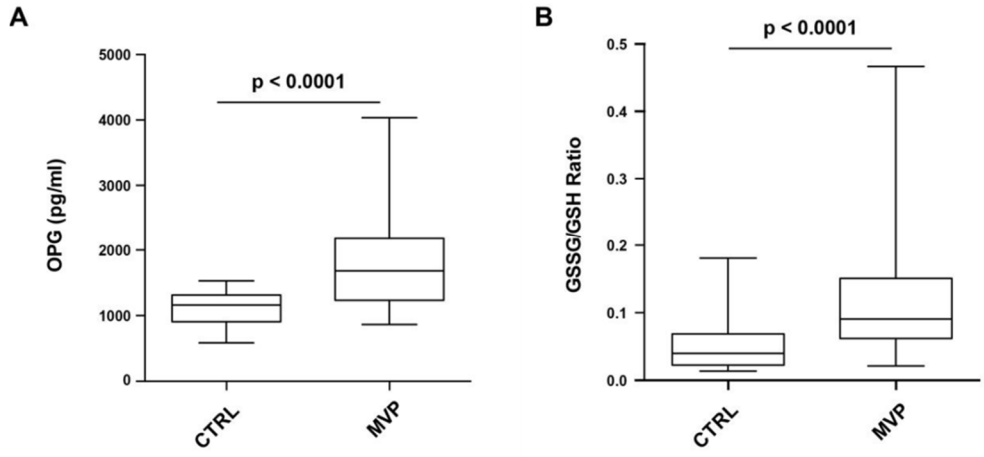

Figure 5.2 Osteoprotegerin and oxidative stress levels. (**A**) Osteoprotegerin (OPG) enzyme-linked immunosorbent assay (ELISA) on plasma samples from control subjects (CTRL) and mitral valve prolapse (MVP) patients. (**B**) Ratio between oxidized (GSSG) and reduced (GSH) form of glutathione as oxidative stress status index in CTRL and MVP patients.

5.4 Clinical predictors of mitral valve prolapse

In order to characterize better OPG as a possible new biomarker, we took into account the conventional cardiovascular risk factors (age, BMI, sex, glucose, total cholesterol - Tot Col-, triglycerides - TG -, low-density lipoprotein – LDL- and high density lipoprotein - HDL) performing a logistic regression method (**Figure 5.3**). We included in the next step only factors with a $p \leq 0.05$ as previously published by *Bursac et al*. [102], indicating a possible correlation with MVP presence. MVP was strongly and independently associated only with BMI ($p = 0.005$). Based on these evaluations and taking into account that BMI [22] levels had already been associated with MVP, we decided to implement a multivariable binary logistic regression model using these parameters.

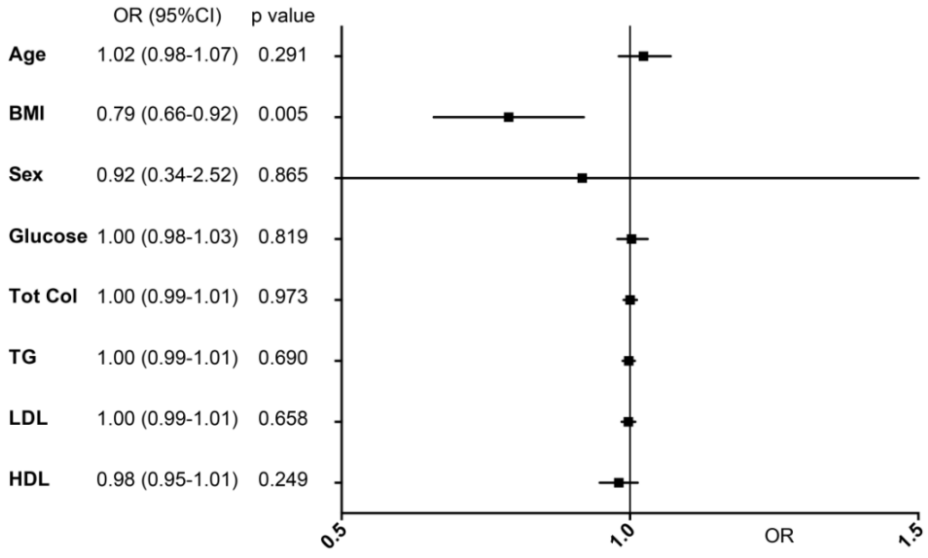

Figure 5.3 Predictors of the presence of mitral valve prolapse. OR, odds ratio; CI, confidence interval; BMI, body mass index; Tot Col, total cholesterol; TG, triglycerides; LDL, low density lipoprotein; HDL, high density lipoprotein.

5.5 Binary logistic regression model

To understand better if OPG and/or GSSG/GSH ratio could be used as potential circulating markers of MVP, we performed a step-wise binary logistic regression model. We also considered BMI levels in order to obtain an improvement in specificity and sensibility. The regression parameters obtained from estimation procedure were $\beta 0 = 1.821$, $\beta 1 = 0.005$, $\beta 2 = 36.031$, $\beta 3 = -0.428$ and the logistic model implemented is described in the Material and Methods section. This model was able to correctly classify 67 samples out of 72 **(Figure 5.4).** In addition, the logistic regression model pointed out an odds ratio of 177.7 (95%CI: 27.8-1136.1; $p<0.0001$) to have MVP for subjects with $p(Y\_i='MVP') > 0.5$.

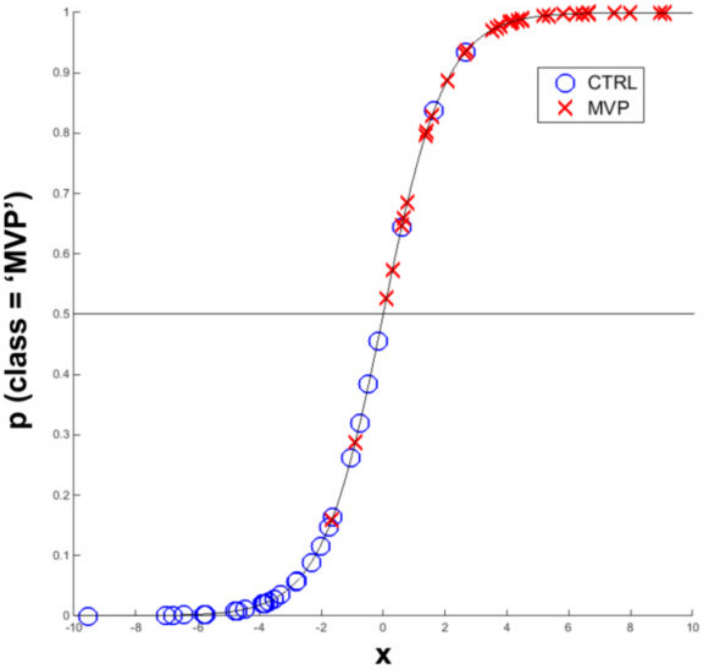

Figure 5.4 Binary logistic regression model. Graph representing the prediction of the best binary logistic regression model.

5.6 Osteoprotegerin as potential circulating marker of MVP

We performed a receiver operator characteristic (ROC) curve to determine if OPG and or GSSG/GSH ratio together with BMI permitted us to identify MVP patients.

As shown in **Figure 5.5A**, OPG and GSSG/GSH ratio had an area under ROC curve of 0.92 (95% CI: 0.86 – 0.98) with $p<0.0001$; but if we combined OPG with GSSG/GSH and BMI we observed accuracy in terms of AUC of 0.95 (95% CI: 0.90 – 0.99) and a sensitivity of 88.4% (95% CI: 74.9-96.1) and a specificity of 86.2% (95% CI: 68.3 -96.1) with $p<0.001$ (**Figure 5.5B**).

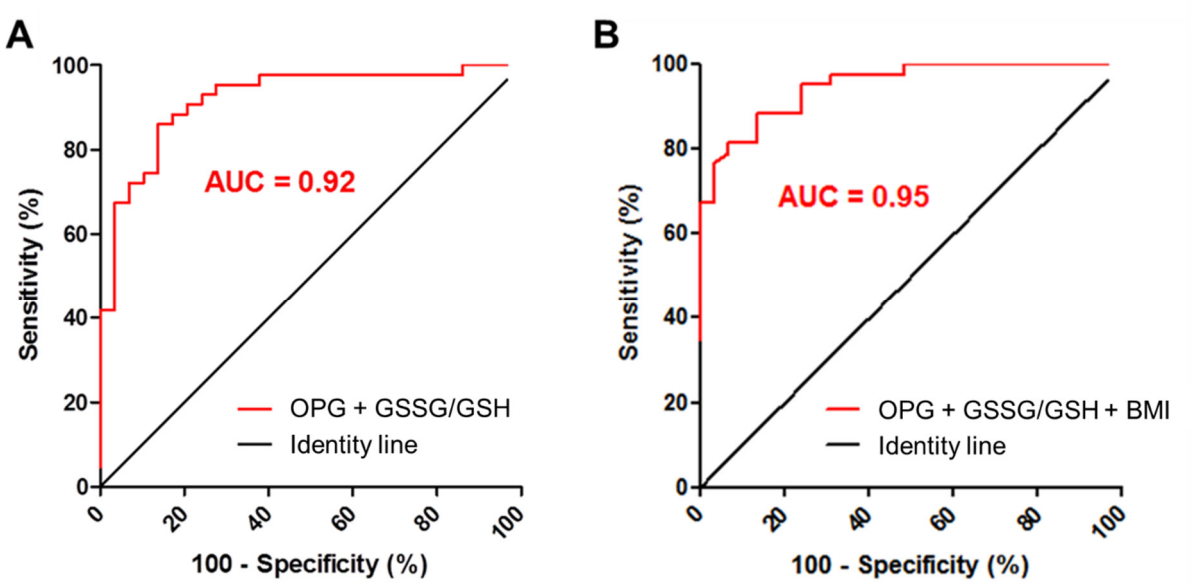

Figure 5.5 Osteoprotegerin combined with oxidative stress and BMI as potential circulating marker of MVP. Receiver operating characteristic (ROC) curves and area under the curve (AUC) of osteoprotegerin (OPG) combined with (**A**) the ratio between oxidized (GSSG) and reduced (GSH) form of glutathione (GSSG/GSH); (**B**) GSSG/GSH and body mass index (BMI). (control subjects n = 29, mitral valve prolapse patients n = 43; $p<0.0001$).

6. DISCUSSION

Mitral valve prolapse (MVP) is a frequent cause of heart failure and mortality. To date, pharmacological treatments are not available and surgical intervention (repair or replacement) is the only successful treatment.

Our results support that endothelial to mesenchymal transition (EndMT) is a possible process involved in the pathogenesis of mitral valve degeneration. In addition, we showed that OPG may be involved in EndMT and, therefore, it could be considered as a new player in the disease progression. OPG is known as a decoy receptor for receptor activator of NF-κB ligand (RANKL) and tumour necrosis factor-related apoptosis-inducing ligand (TRAIL), regulating multiple processes (*i.e.* bone resorption and cell apoptosis). In a recent review, it has been considered the overall knowledge regarding OPG/RANK/TRAIL axis in cardiometabolic disorders [53] and the possibility that OPG evaluation may be considered as a novel biomarker of disease complications and severity [53]. Several studies also described the relationship of OPG with coronary artery syndromes [46-48], aortic valve stenosis [49-51], myocardial infarction [52] and cardiovascular postoperative outcome [103], focusing only on the tumour necrosis factor superfamily.

Interestingly, OPG is not only a decoy receptor but is also able to interact, through its heparin domain, with heparin-sulphate proteoglycans such as syndecan receptors [61]. This family is made up of four isoforms involved in different cellular processes such as apoptosis [61], migration, proliferation [100] and metalloproteinases (MMPs) secretion [104]. Recently, it has been reported that the posterior leaflet thickening, in MVP patients, is due to the formation of new fibrous tissue and extracellular matrix alterations [28]. In particular, MMPs [30, 93], bone morphogenetic protein 4 (BMP4) and VIC over proliferation [33] are involved in MVP progression. We show for the first time that OPG is overexpressed in MVP tissues in comparison to healthy subjects and that VECs are capable of producing and secreting OPG during EndMT. Consequently, OPG interferes with the correct valve endothelial function,

increases collagen deposition, overexpresses BMP4, proteoglycan and MMPs. Therefore, once OPG is upregulated, a vicious circle starts, potentiating valve EndMT, interstitial cell (VIC) activation as well as OPG self-upregulation. Overall, these results suggest a direct involvement of OPG in MVP pathogenesis.

In the clinical practice, 2D-echocardiography is the only reliable clinical tool and circulating biomarkers are not available for the identification of this debilitating pathology. To the best of our knowledge, only a comparative proteomic study on plasma samples from 24 pooled MVP patients with moderate to severe mitral regurgitation (MR), revealed reduced levels of haptoglobin, platelet basic protein, and complement component C4b in the MVP/MR patients as compared to the 24 pooled matched control cases [105]. However, the clinical relevance is unclear, in part because most of the identified biomarkers had moderate area under the receiving operating curve. Furthermore, *Thalji et al.* [56] and *Sainger et al.* [33] identified novel players that could be involved in myxomatous mitral valve degeneration and their data offer novel insights into the pathogenesis of MVP but no circulating biomarkers have been evaluated.

Results of the present work show that circulating OPG and oxidative stress status, measured as ratio between oxidized (GSSG) and reduced (GSH) glutathione forms, are positively associated with severe MR due to MVP. In addition, low-normal range body-mass index (BMI) strongly correlated with the presence of MVP. Based on these premises, we developed a multivariable logistic regression model with OPG, GSSG/GSH ratio and BMI values. This model is able to correctly identify 95% of MVP patients and 90% of control subjects.

Since all patients in the MVP group underwent surgery due to symptoms, we ruled out that left ventricular ejection fraction (LVEF) and heart failure (NYHA classes) were the causes of increased OPG plasma levels and oxidative stress status. Our data supports that severe MR,

due to myxomatous MVP, could be identified through this multivariable binary logistic regression model.

The present study has some limitations: first of all, the exiguous number of enrolled patients and mitral annulus calcification (MAC) as possible confounder. However, only two patients in the MVP group had MAC. Since OPG is involved in many cellular processes, in particular calcification, further studies are needed to address also the possible implication of this molecule not only in patients with MAC but also in those who have mitral valve stenosis. Lastly, all the analysed patients had severe regurgitation due to MVP, however, additional studies are required to evaluate whether this model is able to discriminate mild and moderate regurgitation.

7. CONCLUSIONS

Although mitral valve prolapse is a debilitating disease, no recommended pharmacological treatments are available. Nevertheless, beta-blockers and angiotensin-converting enzyme inhibitors are used to reduce valve mechanical stress reduction, thus slightly delaying the pathological process. Surgical intervention remains the only option when the regurgitation becomes severe or symptoms occur. Additionally, the mechanisms underlying the disease pathogenesis and progression are not fully understood. Therefore, a better characterization of molecular pathways may permit the identification of pharmacological targets capable of delaying or avoiding surgical intervention, allowing patient compliance.

What is the role of osteoprotegerin in mitral valve prolapse?

Considering that endothelial to mesenchymal transition seems to be involved in mitral valve prolapse progression, we implemented an *in vitro* system able to force this process in isolated endothelial cells. In our experimental conditions, endothelial cells produced and secreted osteoprotegerin that, in turn, induced different effects on both endothelial and interstitial cells. In particular, we observed that osteoprotegerin, interacting with syndecan receptors, caused extracellular matrix changes in both cell types. Based on these results we may conclude that osteoprotegerin contributes to myxomatous mitral valve degeneration.

Mitral valve prolapse has a prevalence of over 6% in old patients (≥ 65 years). In addition, considering the aging population and the price of the echocardiographic evaluation, the health system costs may rise if pharmacological treatment or cheaper diagnosis tools are not identified.

Could osteoprotegerin be used as biomarker for mitral valve prolapse?

Our results underline that osteoprotegerin could be considered as a circulating biomarker for mitral valve prolapse. However, it is quite hard to believe that one single protein could discriminate two populations with high specificity and sensitivity. Hence, we combined osteoprotegerin with other markers or clinical variables.

We performed a binary logistic regression model combining osteoprotegerin levels with oxidative stress status and body mass index. This model was able to correctly identify 95% of patients and 90% of control subjects. Finally, this approach could enable the identification of new signatures even for other cardiovascular diseases.

8. REFERENCES

1. Sacks, M.S., W. David Merryman, and D.E. Schmidt, *On the biomechanics of heart valve function.* J Biomech, 2009. **42**(12): p. 1804-24.
2. Cheitlin M.D. and Finkbeiner W.E., *Cardiac Anatomy* in *In Chatterjee K., Anderson M. et al. Cardiology, an illustrated Textbook*2013.
3. Kumar, N., M. Kumar, and C.M. Duran, *A revised terminology for recording surgical findings of the mitral valve.* J Heart Valve Dis, 1995. **4**(1): p. 70-5; discussion 76-7.
4. Carpentier, A.F., et al., *The "physio-ring": an advanced concept in mitral valve annuloplasty.* Ann Thorac Surg, 1995. **60**(5): p. 1177-85; discussion 1185-6.
5. Sonnenblick, E.H., et al., *An intrinsic neuromuscular basis for mitral valve motion in the dog.* Circ Res, 1967. **21**(1): p. 9-15.
6. Marron, K., et al., *Innervation of human atrioventricular and arterial valves.* Circulation, 1996. **94**(3): p. 368-75.
7. Filip, D.A., A. Radu, and M. Simionescu, *Interstitial cells of the heart valves possess characteristics similar to smooth muscle cells.* Circ Res, 1986. **59**(3): p. 310-20.
8. Grande-Allen, K.J., et al., *Glycosaminoglycans and proteoglycans in normal mitral valve leaflets and chordae: association with regions of tensile and compressive loading.* Glycobiology, 2004. **14**(7): p. 621-33.
9. Dal-Bianco, J.P., et al., *Active adaptation of the tethered mitral valve: insights into a compensatory mechanism for functional mitral regurgitation.* Circulation, 2009. **120**(4): p. 334-42.
10. Levine, R.A., et al., *Mitral valve disease--morphology and mechanisms.* Nat Rev Cardiol, 2015. **12**(12): p. 689-710.
11. Delling, F.N. and R.S. Vasan, *Epidemiology and pathophysiology of mitral valve prolapse: new insights into disease progression, genetics, and molecular basis.* Circulation, 2014. **129**(21): p. 2158-70.
12. Kunzelman, K.S., et al., *Finite element analysis of the mitral valve.* J Heart Valve Dis, 1993. **2**(3): p. 326-40.
13. Horne, T.E., et al., *Dynamic Heterogeneity of the Heart Valve Interstitial Cell Population in Mitral Valve Health and Disease.* J Cardiovasc Dev Dis, 2015. **2**(3): p. 214-232.
14. Shapero, K., et al., *Reciprocal interactions between mitral valve endothelial and interstitial cells reduce endothelial-to-mesenchymal transition and myofibroblastic activation.* J Mol Cell Cardiol, 2015. **80**: p. 175-85.

15. Tao, G., J.D. Kotick, and J. Lincoln, *Heart valve development, maintenance, and disease: the role of endothelial cells.* Curr Top Dev Biol, 2012. **100**: p. 203-32.
16. Butcher, J.T. and R.M. Nerem, *Valvular endothelial cells regulate the phenotype of interstitial cells in co-culture: effects of steady shear stress.* Tissue Eng, 2006. **12**(4): p. 905-15.
17. Bosse, K., et al., *Endothelial nitric oxide signaling regulates Notch1 in aortic valve disease.* J Mol Cell Cardiol, 2013. **60**: p. 27-35.
18. Nishimura, R.A., et al., *2014 AHA/ACC Guideline for the Management of Patients With Valvular Heart Disease: a report of the American College of Cardiology/American Heart Association Task Force on Practice Guidelines.* Circulation, 2014. **129**(23): p. e521-643.
19. Vahanian, A., et al., *Guidelines on the management of valvular heart disease (version 2012).* Eur Heart J, 2012. **33**(19): p. 2451-96.
20. Abramowitz, Y., et al., *Mitral Annulus Calcification.* J Am Coll Cardiol, 2015. **66**(17): p. 1934-41.
21. Olson, L.J., et al., *Surgical pathology of the mitral valve: a study of 712 cases spanning 21 years.* Mayo Clin Proc, 1987. **62**(1): p. 22-34.
22. Freed, L.A., et al., *Prevalence and clinical outcome of mitral-valve prolapse.* N Engl J Med, 1999. **341**(1): p. 1-7.
23. Boudoulas, K.D. and H. Boudoulas, *Floppy mitral valve (FMV)/mitral valve prolapse (MVP) and the FMV/MVP syndrome: pathophysiologic mechanisms and pathogenesis of symptoms.* Cardiology, 2013. **126**(2): p. 69-80.
24. Barlow, J.B. and W.A. Pocock, *The significance of late systolic murmurs and mid-late systolic clicks.* Md State Med J, 1963. **12**: p. 76-7.
25. Boudoulas, K.D. and H. Boudoulas, *Floppy mitral valve and mitral valve prolapse: lack of precise definition (the Tower of Babel syndrome).* Cardiology, 2011. **118**(2): p. 93-6.
26. Davies, M.J., B.P. Moore, and M.V. Braimbridge, *The floppy mitral valve. Study of incidence, pathology, and complications in surgical, necropsy, and forensic material.* Br Heart J, 1978. **40**(5): p. 468-81.
27. Wooley, C.F., et al., *The floppy, myxomatous mitral valve, mitral valve prolapse, and mitral regurgitation.* Prog Cardiovasc Dis, 1991. **33**(6): p. 397-433.
28. Roberts, W.C., et al., *Gross and histological features of excised portions of posterior mitral leaflet in patients having operative repair of mitral valve prolapse and comments*

on the concept of missing (= ruptured) chordae tendineae. J Am Coll Cardiol, 2014. **63**(16): p. 1667-74.

29. Akhtar, S., K.M. Meek, and V. James, *Ultrastructure abnormalities in proteoglycans, collagen fibrils, and elastic fibers in normal and myxomatous mitral valve chordae tendineae.* Cardiovasc Pathol, 1999. **8**(4): p. 191-201.
30. Rabkin, E., et al., *Activated interstitial myofibroblasts express catabolic enzymes and mediate matrix remodeling in myxomatous heart valves.* Circulation, 2001. **104**(21): p. 2525-32.
31. Rabkin-Aikawa, E., et al., *Dynamic and reversible changes of interstitial cell phenotype during remodeling of cardiac valves.* J Heart Valve Dis, 2004. **13**(5): p. 841-7.
32. Grande-Allen, K.J., et al., *Glycosaminoglycan profiles of myxomatous mitral leaflets and chordae parallel the severity of mechanical alterations.* J Am Coll Cardiol, 2003. **42**(2): p. 271-7.
33. Sainger, R., et al., *Human myxomatous mitral valve prolapse: role of bone morphogenetic protein 4 in valvular interstitial cell activation.* J Cell Physiol, 2012. **227**(6): p. 2595-604.
34. Rizzo, S., et al., *TGF-beta1 pathway activation and adherens junction molecular pattern in nonsyndromic mitral valve prolapse.* Cardiovasc Pathol, 2015. **24**(6): p. 359-67.
35. Carpentier, A., et al., *Reconstructive surgery of mitral valve incompetence: ten-year appraisal.* J Thorac Cardiovasc Surg, 1980. **79**(3): p. 338-48.
36. Barlow, J.B. and C.K. Bosman, *Aneurysmal protrusion of the posterior leaflet of the mitral valve. An auscultatory-electrocardiographic syndrome.* Am Heart J, 1966. **71**(2): p. 166-78.
37. Anyanwu, A.C. and D.H. Adams, *Etiologic classification of degenerative mitral valve disease: Barlow's disease and fibroelastic deficiency.* Semin Thorac Cardiovasc Surg, 2007. **19**(2): p. 90-6.
38. Adams, D.H., R. Rosenhek, and V. Falk, *Degenerative mitral valve regurgitation: best practice revolution.* Eur Heart J, 2010. **31**(16): p. 1958-66.
39. Fornes, P., et al., *Correlation between clinical and histologic patterns of degenerative mitral valve insufficiency: a histomorphometric study of 130 excised segments.* Cardiovasc Pathol, 1999. **8**(2): p. 81-92.

40. Eriksson, M.J., et al., *Mitral annular disjunction in advanced myxomatous mitral valve disease: echocardiographic detection and surgical correction.* J Am Soc Echocardiogr, 2005. **18**(10): p. 1014-22.
41. Willis M., Homeister J.W., and S. J.R., *Cellular and Molecular Pathobiology of Cardiovascular Disease*2013.
42. Bolling, S.F., et al., *Intermediate-term outcome of mitral reconstruction in cardiomyopathy.* J Thorac Cardiovasc Surg, 1998. **115**(2): p. 381-6; discussion 387-8.
43. Asgar, A.W., M.J. Mack, and G.W. Stone, *Secondary mitral regurgitation in heart failure: pathophysiology, prognosis, and therapeutic considerations.* J Am Coll Cardiol, 2015. **65**(12): p. 1231-48.
44. Wylie-Sears, J., et al., *Mitral valve endothelial cells with osteogenic differentiation potential.* Arterioscler Thromb Vasc Biol, 2011. **31**(3): p. 598-607.
45. Bischoff, J. and E. Aikawa, *Progenitor cells confer plasticity to cardiac valve endothelium.* J Cardiovasc Transl Res, 2011. **4**(6): p. 710-9.
46. Hermann-Arnhof, K.M., et al., *Initially elevated osteoprotegerin serum levels may predict a perioperative myocardial lesion in patients undergoing coronary artery bypass grafting.* Critical Care Medicine, 2006. **34**(1): p. 76-80.
47. Omland, T., et al., *Circulating osteoprotegerin levels and long-term prognosis in patients with acute coronary syndromes.* J Am Coll Cardiol, 2008. **51**(6): p. 627-33.
48. Tousoulis, D., et al., *Serum osteoprotegerin and osteopontin levels are associated with arterial stiffness and the presence and severity of coronary artery disease.* Int J Cardiol, 2013. **167**(5): p. 1924-8.
49. Kaden, J.J., et al., *Receptor activator of nuclear factor kappaB ligand and osteoprotegerin regulate aortic valve calcification.* J Mol Cell Cardiol, 2004. **36**(1): p. 57-66.
50. Borowiec, A., et al., *Osteoprotegerin in patients with degenerative aortic stenosis and preserved left-ventricular ejection fraction.* J Cardiovasc Med (Hagerstown), 2015. **16**(6): p. 444-50.
51. Dahl, J.S., et al., *Relation of osteoprotegerin in severe aortic valve stenosis to postoperative outcome and left ventricular function.* American Journal of Cardiology, 2013. **112**(9): p. 1433-8.

52. Margonato, A., et al., *Role of plaque calcification regulators osteoprotegerin and matrix Gla-proteins in stable angina and acute myocardial infarction.* J Cardiovasc Med (Hagerstown), 2015. **16**(3): p. 156-62.
53. Perez de Ciriza, C., A. Lawrie, and N. Varo, *Osteoprotegerin in Cardiometabolic Disorders.* Int J Endocrinol, 2015. **2015**: p. 564934.
54. Avignon, A., et al., *Osteoprotegerin: a novel independent marker for silent myocardial ischemia in asymptomatic diabetic patients.* Diabetes Care, 2007. **30**(11): p. 2934-9.
55. Gordin, D., et al., *Osteoprotegerin is an independent predictor of vascular events in Finnish adults with type 1 diabetes.* Diabetes Care, 2013. **36**(7): p. 1827-33.
56. Thalji, N.M., et al., *Nonbiased Molecular Screening Identifies Novel Molecular Regulators of Fibrogenic and Proliferative Signaling in Myxomatous Mitral Valve Disease.* Circ Cardiovasc Genet, 2015. **8**(3): p. 516-28.
57. Hagler, M.A., et al., *TGF-beta signalling and reactive oxygen species drive fibrosis and matrix remodelling in myxomatous mitral valves.* Cardiovasc Res, 2013. **99**(1): p. 175-84.
58. Thirunavukkarasu, K., et al., *Stimulation of osteoprotegerin (OPG) gene expression by transforming growth factor-beta (TGF-beta). Mapping of the OPG promoter region that mediates TGF-beta effects.* J Biol Chem, 2001. **276**(39): p. 36241-50.
59. Zannettino, A.C., et al., *Osteoprotegerin (OPG) is localized to the Weibel-Palade bodies of human vascular endothelial cells and is physically associated with von Willebrand factor.* J Cell Physiol, 2005. **204**(2): p. 714-23.
60. Schoppet, M., et al., *Crystallizing nanoparticles derived from vascular smooth muscle cells contain the calcification inhibitor osteoprotegerin.* Biochem Biophys Res Commun, 2011. **407**(1): p. 103-7.
61. Kim, J.Y., et al., *Osteoprotegerin causes apoptosis of endothelial progenitor cells by induction of oxidative stress.* Arthritis Rheum, 2013. **65**(8): p. 2172-82.
62. Lambaerts, K., S.A. Wilcox-Adelman, and P. Zimmermann, *The signaling mechanisms of syndecan heparan sulfate proteoglycans.* Curr Opin Cell Biol, 2009. **21**(5): p. 662-9.
63. Levine, R.A., et al., *Reconsideration of echocardiographic standards for mitral valve prolapse: lack of association between leaflet displacement isolated to the apical four chamber view and independent echocardiographic evidence of abnormality.* J Am Coll Cardiol, 1988. **11**(5): p. 1010-9.

64. Zoghbi, W.A., et al., *Recommendations for evaluation of the severity of native valvular regurgitation with two-dimensional and Doppler echocardiography.* J Am Soc Echocardiogr, 2003. **16**(7): p. 777-802.
65. Filho, A.S., et al., *Does the association between mitral valve prolapse and panic disorder really exist?* Prim Care Companion J Clin Psychiatry, 2008. **10**(1): p. 38-47.
66. Lang, R.M., et al., *EAE/ASE recommendations for image acquisition and display using three-dimensional echocardiography.* J Am Soc Echocardiogr, 2012. **25**(1): p. 3-46.
67. Hulka, B.S. and T. Wilcosky, *Biological markers in epidemiologic research.* Arch Environ Health, 1988. **43**(2): p. 83-9.
68. Naylor, S., *Biomarkers: current perspectives and future prospects.* Expert Rev Mol Diagn, 2003. **3**(5): p. 525-9.
69. Deroyer, C., et al., *New biomarkers for primary mitral regurgitation.* Clin Proteomics, 2015. **12**: p. 25.
70. Cavalca, V., et al., *Oxidative stress and nitric oxide pathway in adult patients who are candidates for cardiac surgery: patterns and differences.* Interact Cardiovasc Thorac Surg, 2013. **17**(6): p. 923-30.
71. Hulanicka, M., et al., *Plasma miRNAs as potential biomarkers of chronic degenerative valvular disease in Dachshunds.* BMC Vet Res, 2014. **10**: p. 205.
72. Li, Q., et al., *Expression Profiling of Circulating MicroRNAs in Canine Myxomatous Mitral Valve Disease.* Int J Mol Sci, 2015. **16**(6): p. 14098-108.
73. Nagatsu, M., et al., *Bradycardia and the role of beta-blockade in the amelioration of left ventricular dysfunction.* Circulation, 2000. **101**(6): p. 653-9.
74. Gammie, J.S., et al., *Trends in mitral valve surgery in the United States: results from the Society of Thoracic Surgeons Adult Cardiac Surgery Database.* Ann Thorac Surg, 2009. **87**(5): p. 1431-7; discussion 1437-9.
75. Enriquez-Sarano, M., et al., *Valve repair improves the outcome of surgery for mitral regurgitation. A multivariate analysis.* Circulation, 1995. **91**(4): p. 1022-8.
76. Gillinov, A.M., et al., *Valve repair versus valve replacement for degenerative mitral valve disease.* J Thorac Cardiovasc Surg, 2008. **135**(4): p. 885-93, 893 e1-2.
77. Suri, R.M., et al., *Survival advantage and improved durability of mitral repair for leaflet prolapse subsets in the current era.* Ann Thorac Surg, 2006. **82**(3): p. 819-26.
78. Zhou, Y.X., et al., *Long-term outcomes following repair or replacement in degenerative mitral valve disease.* Thorac Cardiovasc Surg, 2010. **58**(7): p. 415-21.

79. Daneshmand, M.A., et al., *Mitral valve repair for degenerative disease: a 20-year experience.* Ann Thorac Surg, 2009. **88**(6): p. 1828-37.
80. LaPar, D.J., et al., *Does urgent or emergent status influence choice in mitral valve operations? An analysis of outcomes from the Virginia Cardiac Surgery Quality Initiative.* Ann Thorac Surg, 2010. **90**(1): p. 153-60.
81. Akins, C.W., et al., *Mitral valve reconstruction versus replacement for degenerative or ischemic mitral regurgitation.* Ann Thorac Surg, 1994. **58**(3): p. 668-75; discussion 675-6.
82. Habib, G., F. Thuny, and J.F. Avierinos, *Prosthetic valve endocarditis: current approach and therapeutic options.* Prog Cardiovasc Dis, 2008. **50**(4): p. 274-81.
83. Seeburger, J., et al., *Chordae replacement versus resection for repair of isolated posterior mitral leaflet prolapse: a egalite.* Ann Thorac Surg, 2009. **87**(6): p. 1715-20.
84. Suri, R.M., et al., *Effect of Recurrent Mitral Regurgitation Following Degenerative Mitral Valve Repair: Long-Term Analysis of Competing Outcomes.* J Am Coll Cardiol, 2016. **67**(5): p. 488-98.
85. Guy, T.S. and A.C. Hill, *Mitral valve prolapse.* Annu Rev Med, 2012. **63**: p. 277-92.
86. Nishimura, R.A., et al., *Mitral valve disease--current management and future challenges.* Lancet, 2016. **387**(10025): p. 1324-34.
87. Mirabel, M., et al., *What are the characteristics of patients with severe, symptomatic, mitral regurgitation who are denied surgery?* Eur Heart J, 2007. **28**(11): p. 1358-65.
88. Feldman, T., et al., *Percutaneous repair or surgery for mitral regurgitation.* N Engl J Med, 2011. **364**(15): p. 1395-406.
89. Feldman, T., et al., *Randomized Comparison of Percutaneous Repair and Surgery for Mitral Regurgitation: 5-Year Results of EVEREST II.* J Am Coll Cardiol, 2015. **66**(25): p. 2844-54.
90. Acker, M.A., et al., *Mitral-valve repair versus replacement for severe ischemic mitral regurgitation.* N Engl J Med, 2014. **370**(1): p. 23-32.
91. Goldstein, D., et al., *Two-Year Outcomes of Surgical Treatment of Severe Ischemic Mitral Regurgitation.* N Engl J Med, 2016. **374**(4): p. 344-53.
92. Singh, R.G., et al., *Severe mitral regurgitation due to mitral valve prolapse: risk factors for development, progression, and need for mitral valve surgery.* American Journal of Cardiology, 2000. **85**(2): p. 193-8.

93. Mahimkar, R., et al., *Cardiac transgenic matrix metalloproteinase-2 expression induces myxomatous valve degeneration: a potential model of mitral valve prolapse disease.* Cardiovasc Pathol, 2009. **18**(5): p. 253-61.
94. Poggio, P., et al., *Osteopontin-CD44v6 interaction mediates calcium deposition via phospho-Akt in valve interstitial cells from patients with noncalcified aortic valve sclerosis.* Arterioscler Thromb Vasc Biol, 2014. **34**(9): p. 2086-94.
95. Squellerio, I., et al., *Direct glutathione quantification in human blood by LC-MS/MS: comparison with HPLC with electrochemical detection.* J Pharm Biomed Anal, 2012. **71**: p. 111-8.
96. Zimmermann, P. and G. David, *The syndecans, tuners of transmembrane signaling.* FASEB J, 1999. **13 Suppl**: p. S91-S100.
97. Keller-Pinter, A., et al., *Syndecan-4 promotes cytokinesis in a phosphorylation-dependent manner.* Cell Mol Life Sci, 2010. **67**(11): p. 1881-94.
98. Benslimane-Ahmim, Z., et al., *Mechanistic study of the proangiogenic effect of osteoprotegerin.* Angiogenesis, 2013. **16**(3): p. 575-93.
99. Feng, Z.Y., et al., *Osteoprotegerin promotes the proliferation of chondrocytes and affects the expression of ADAMTS-5 and TIMP-4 through MEK/ERK signaling.* Mol Med Rep, 2013. **8**(6): p. 1669-79.
100. Candido, R., et al., *Human full-length osteoprotegerin induces the proliferation of rodent vascular smooth muscle cells both in vitro and in vivo.* J Vasc Res, 2010. **47**(3): p. 252-61.
101. Gupta, V., et al., *Abundance and location of proteoglycans and hyaluronan within normal and myxomatous mitral valves.* Cardiovasc Pathol, 2009. **18**(4): p. 191-7.
102. Bursac, Z., et al., *Purposeful selection of variables in logistic regression.* Source Code Biol Med, 2008. **3**: p. 17.
103. Venuraju, S.M., et al., *Osteoprotegerin as a predictor of coronary artery disease and cardiovascular mortality and morbidity.* J Am Coll Cardiol, 2010. **55**(19): p. 2049-61.
104. Moran, C.S., et al., *Association of osteoprotegerin with human abdominal aortic aneurysm progression.* Circulation, 2005. **111**(23): p. 3119-25.
105. Tan, H.T., et al., *Proteomics discovery of biomarkers for mitral regurgitation caused by mitral valve prolapse.* J Proteomics, 2013. **94**: p. 337-45.

APPENDIX A

Table A1. ***Primer list.***

Primers		
GAPDH	Fw	ACA TCG CTC AGA CAC CAT G
	Rv	TGT AGT TGA GGT CAA TGA AGG G
SMA	Fw	AGA GTT ACG AGT TGC CTG ATG
	Rv	CTG TTG TAG GTG GTT TCA TGG A
COL1A1	Fw	GGA CAC AGA GGT TTC AGT GG
	Rv	CCA GTA GCA CCA TCA TTT CC
COL3A1	Fw	AGC TAC GGC AAT CCT GAA CT
	Rv	GGG CCT TCT TTA CAT TTC CA
BMP4	Fw	GAG CCT TTC CAG CAA GTT TG
	Rv	CCA TCA GCA TTC GGT TAC CA
SDC1	Fw	CTA CTA ATT TGC CCC CTG AAG A
	Rv	GTC TGC TGT GAC AAG GTG AT
SDC2	Fw	GTC TCA GAT TGA CCT TAC CAA GT
	Rv	ATT GCA CCA TGA CAG CTA CA
SDC3	Fw	GAG CCT GAC ATC CCT GAG A
	Rv	GGA TTG TGG TCA GGA AGG T
SDC4	Fw	GCA GCA ACA TCT TTG AGA GAA C
	Rv	GGT ACA TGA GCA GTA GGA TCA G
FSP1	Fw	CTC TAC AAC CCT CTC TCC TCA
	Rv	GTT GAG CTT GAA CTT GTC ACC
BGN	Fw	CAC CGG ACA GAT AGA CGT G
	Rv	CCA CAT GGC GGA TGG AC
VCAN	Fw	AAC TTC CTA CGT ATG CAC CTG
	Rv	AAG TGG CTC CAT TAC GAC AG
MMP2	Fw	TCC ACC ACC TAC AAC TTT GAG
	Rv	GTG CAG CTG TCA TAG GAT GT
OPG	Fw	AAA CAG TGA ATC AAC TCA AAA ATG TG
	Rv	CTA CCA AGA CAC TAA GCC AGT
Alpha V	Fw	ACT CTT AGC TGG TCT TCG TTT C
	Rv	TGT GAG ATA CAA CTG GGC TTA C
Beta 3	Fw	CAA GTG TGA ATG TGG CAG C
	Rv	TTT TCG TCA TGT AGG GCT CC

Fw = forward; Rv = reverse.

Table A2. ***Digital PCR of valve endothelial cells.***

Chip	# of Neg (VIC)	# of Neg (FAM)	# qualified by QT	# of Filled
VEC5 SDC1.eds	1397	15735	15778	17025
VEC8 SDC1.eds	3094	16069	16843	18350
VEC7 SDC1.eds	5022	17067	17460	18814
VEC2 SDC1.eds	2897	15283	16292	17936
VEC3 SDC1.eds	2291	16896	17545	18656
VEC9 SDC1.eds	516	17595	17638	18520
VEC6 SDC1.eds	2689	16892	18460	19346
VEC4 SDC2.eds	2623	14415	14547	17461
VEC3 SDC2.eds	3269	17149	17267	17938
VEC8 SDC2.eds	3764	17599	17676	19066
VEC1 SDC2.eds	1395	16681	16809	17675
VEC2 SDC2.eds	713	16161	16374	17834
VEC5 SDC2.eds	1648	17678	17939	19163
VEC7 SDC2.eds	1546	16826	16996	18033
VEC6 SDC2.eds	3315	17465	17515	18520
VEC9 SDC2.eds	2581	17368	17562	18522
VEC1 SDC3.eds	1684	16756	17235	18420
VEC4 SDC3.eds	3593	16948	17539	18155
VEC2 SDC3.eds	2713	15469	15972	17664
VEC5 SDC3.eds	4009	16191	17216	18092
VEC3 SDC3.eds	5067	16767	17411	18323
VEC5 SDC4.eds	4748	17878	18359	19236
VEC3 SDC4.eds	1916	17606	17987	18857
VEC4 SDC4.eds	3649	17670	17851	18816
VEC2 SDC4.eds	1777	17194	17500	18072
VEC1 SDC4.eds	1880	17971	18332	19043

VEC = valve endothelial cell; SDC = syndecan.

The number after VEC represents the population, while the number after SDC represent the specific receptor.

Table A3. ***Digital PCR of valve interstitial cells.***

Chip	# of Neg (VIC)	# of Neg (FAM)	# qualified by QT	# of Filled
VIC1 SDC1.eds	7476	16449	16672	18409
VIC2 SDC1.eds	10627	17904	17940	18594
VIC3 SDC1.eds	1538	15934	15987	18497
VIC3 SDC2.eds	6030	14550	17660	18423
VIC2 SDC2.eds	11134	16927	18043	18688
VIC1 SDC2.eds	5012	15924	17730	18385
VIC1 SDC3.eds	7608	16005	17733	18318
VIC3 SDC3.eds	8525	16835	17735	18627
VIC2 SDC3.eds	10891	17314	17736	18495
VIC3 SDC4.eds	5801	17085	17805	18647
VIC1 SDC4.eds	4280	15692	17438	18198
VIC2 SDC4.eds	7639	17086	17381	18404

VIC = valve interstitial cell; SDC = syndecan.

The number after VIC represents the population, while the number after SDC represent the specific receptor.